DESY 11-030
Edinburgh 2011/09
LTH 909
February 25, 2011

Flavour blindness and patterns of flavour symmetry breaking in lattice simulations of up, down and strange quarks

W. Bietenholz[a], V. Bornyakov[b], M. Göckeler[c], R. Horsley[d], W. G. Lockhart[e], Y. Nakamura[f], H. Perlt[g], D. Pleiter[h], P. E. L. Rakow[e], G. Schierholz[ci], A. Schiller[g], T. Streuer[c], H. Stüben[j], F. Winter[d] and J. M. Zanotti[d]

– QCDSF-UKQCD Collaboration –

[a] Instituto de Ciencias Nucleares, Universidad Autónoma de México, A.P. 70-543, C.P. 04510 Distrito Federal, Mexico

[b] Institute for High Energy Physics, 142281 Protovino, Russia and Institute of Theoretical and Experimental Physics, 117259 Moscow, Russia

[c] Institut für Theoretische Physik, Universität Regensburg, 93040 Regensburg, Germany

[d] School of Physics and Astronomy, University of Edinburgh, Edinburgh EH9 3JZ, UK

[e] Theoretical Physics Division, Department of Mathematical Sciences, University of Liverpool, Liverpool L69 3BX, UK

[f] Center for Computational Sciences, University of Tsukuba, Tsukuba, Ibaraki 305-8577, Japan

[g] Institut für Theoretische Physik, Universität Leipzig, 04109 Leipzig, Germany

[h] Deutsches Elektronen-Synchrotron DESY, 15738 Zeuthen, Germany

[i] Deutsches Elektronen-Synchrotron DESY, 22603 Hamburg, Germany

[j] Konrad-Zuse-Zentrum für Informationstechnik Berlin, 14195 Berlin, Germany

Abstract

QCD lattice simulations with 2+1 flavours typically start at rather large up-down and strange quark masses and extrapolate first the strange quark mass to its physical value and then the up-down quark mass. An alternative method of tuning the quark masses is discussed here in which the singlet quark mass is kept fixed, which ensures that the kaon always has mass less than the physical kaon mass. Using group theory the possible quark mass polynomials for a Taylor expansion about the flavour symmetric line are found, first for the general $1 + 1 + 1$ flavour case and then for the $2 + 1$ flavour case (when two quark flavours are mass degenerate). These enable highly constrained fits to be used in the extrapolation of hadrons to the physical pion mass. Numerical results for the $2 + 1$ flavour case confirm the usefulness of this expansion and an extrapolation to the physical pion mass gives hadron mass values to within a few percent of their experimental values. Singlet quantities remain constant which allows the lattice spacing to be determined from hadron masses (without necessarily being at the physical point). Furthermore an extension of this programme to include partially quenched results is also given.

1 Introduction

The QCD interaction is flavour blind. Neglecting electromagnetic and weak interactions, the only difference between quark flavours comes from the quark mass matrix, which originates from the coupling to the Higgs particle. We investigate here how flavour blindness constrains hadron masses after flavour $SU(3)$ is broken by the mass difference between the strange and light quarks, to help us extrapolate $2+1$ flavour lattice data to the physical point. (By $2+1$ we mean that the u and d quarks are mass degenerate.)

We have our best theoretical understanding when all 3 quark flavours have the same masses (because we can use the full power of flavour $SU(3)$); nature presents us with just one instance of the theory, with $m_s^R/m_l^R \approx 25$ (where ^{R} denotes the renormalised mass). We are interested in interpolating between these two cases.

We consider possible behaviours near the symmetric point, and find that flavour blindness is particularly helpful if we approach the physical point, denoted by (m_l^{R*}, m_s^{R*}), along a path in the $(m_l^R$–$m_s^R)$ plane starting at a point on the $SU(3)$ flavour symmetric line $(m_l^R = m_s^R)$ and holding the sum of the quark masses $m_u^R + m_d^R + m_s^R \equiv 2m_l^R + m_s^R \equiv 3\overline{m}$ constant, [1], as sketched in Fig. 1. The usual procedure (path) is to estimate the physical strange quark mass and

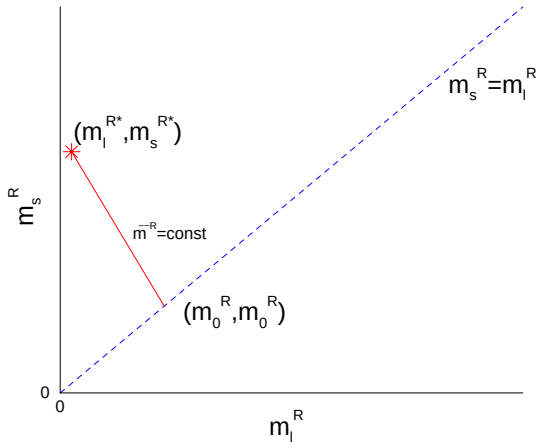

Figure 1: Sketch of the path (red, solid line) in the (m_l^R, m_s^R) plane to the physical point denoted by (m_l^{R*}, m_s^{R*}). The dashed diagonal line is the $SU(3)$-symmetric line.

then try to keep it fixed, i.e. $m_s^R =$ constant, as the light quark mass is reduced to its physical value. However the problem is that the kaon mass is always larger than its physical value. By choosing instead a path such that the singlet quark mass is kept fixed, this has the advantage that we can vary both quark masses over a wide range, with the kaon mass always being lighter than its physical value along the entire trajectory. Starting from the symmetric point when masses are

degenerate is particularly useful for strange quark physics as we can track the development of the strange quark mass. Also if we extend our measurements beyond the symmetric point we can investigate a world with heavy up-down quarks and a lighter strange quark.

The plan of this article is as follows. Before considering the $2+1$ quark flavour case, we consider the more general $1+1+1$ case in section 2. This also includes a discussion of the renormalisation of quark masses for non-chiral fermions. Keeping the singlet quark mass constant constrains the extrapolation and in particular it is shown in this section that flavour singlet quantities remain constant to leading order when extrapolating from a flavour symmetric point. This motivates investigating possible quark mass polynomials – we are able to classify them here to third order in the quark masses under the $SU(3)$ and S_3 (flavour) groups.

In section 3 we specialise to $2+1$ flavours and give quark mass expansions to second order in the quark masses for the pseudoscalar and vector octets and baryon octet and decuplet. The relation of this expansion to chiral perturbation theory is discussed in section 4. In section 5 we extend the formalism to the partially quenched case (when the valence quarks of a hadron do not have to have the same mass as the sea quarks). This is potentially useful as the same expansion coefficients occur, which could allow a cheaper determination of them. We then turn to more specific lattice considerations in section 7 with emphasis on clover fermions (i.e. non-chiral fermions) used here. This is followed by section 8, which first gives numerical results for the constant singlet quark mass results used here. Flavour singlet quantities prove to be a good way of defining the scale and the consistency of some choices is discussed. We also investigate possible finite size effects. Finally in section 9 the numerical results for the hadron mass spectrum are presented in the form of a series of 'fan' plots where the various masses fan out from their common value at the symmetric point. Some conclusions are given in section 10. Several Appendices provide some group theory background for this article, discuss the action used here and give tables of the hadron masses found.

2 Theory: $1+1+1$ flavours

Our strategy is to start from a point with all 3 sea quark masses equal,

$$m_u^R = m_d^R = m_s^R \equiv m_0^R \,, \tag{1}$$

and extrapolate towards the physical point, $(m_u^{R*}, m_d^{R*}, m_s^{R*})$, keeping the average sea quark mass

$$\overline{m}^R = \tfrac{1}{3}(m_u^R + m_d^R + m_s^R) \tag{2}$$

constant. For this trajectory to reach the physical point we have to start at a point where $m_0^R \approx \frac{1}{3} m_s^{R*}$. As we approach the physical point, the u and d quarks

become lighter, but the s quark becomes heavier. Pions are decreasing in mass, but K and η increase in mass as we approach the physical point.

2.1 Singlet and non-singlet renormalisation

Before developing the theory, we first briefly comment on the renormalisation of the quark mass. While for chiral fermions the renormalised quark mass is directly proportional to the bare quark mass, $m_q^R = Z_m m_q$, the problem, at least for Wilson-like fermions which have no chiral symmetry, is that singlet and non-singlet quark mass can renormalise differently [2, 3][1]

$$m_q^R = Z_m^{NS}(m_q - \overline{m}) + Z_m^S \overline{m}\,, \qquad q = u, d, s\,, \tag{3}$$

where m_q are the bare quark masses,

$$\overline{m} = \tfrac{1}{3}(m_u + m_d + m_s)\,, \tag{4}$$

Z_m^{NS} is the non-singlet renormalisation constant, and Z_m^S is the singlet renormalisation constant (both in scheme R). It is often convenient to re-write eq. (3) as

$$m_q^R = Z_m^{NS}(m_q + \alpha_Z \overline{m})\,, \tag{5}$$

where

$$\alpha_Z = r_m - 1\,, \quad r_m = \frac{Z_m^S}{Z_m^{NS}} \tag{6}$$

represents the fractional difference between the renormalisation constants. (Numerically we later see that this factor α_Z is $\sim O(1)$, and is thus non-negligible.) This then gives

$$\overline{m}^R = Z_m^{NS}(1 + \alpha_Z)\overline{m}\,. \tag{7}$$

This means that even for Wilson-type actions it does not matter whether we keep the bare or renormalised average sea quark mass constant. Obviously this also holds for a reference point on the flavour symmetric line, i.e.

$$m_0^R = Z_m^S m_0 = Z_m^{NS}(1 + \alpha_Z) m_0\,. \tag{8}$$

Furthermore introducing the notation

$$\delta m_q^R \equiv m_q^R - m_0^R\,, \qquad \delta m_q \equiv m_q - m_0\,, \qquad q = u, d, s\,, \tag{9}$$

for both renormalised and bare quark masses, we find that

$$\delta m_q^R = Z_m^{NS}\, \delta m_q\,. \tag{10}$$

[1] Perturbative computations showing this effect, which starts at the two-loop order, are given in [4, 5].

So by keeping the singlet mass constant we avoid the need to use two different Zs and as we will be considering expansions about the flavour symmetric point, they will be similar using either the renormalised or bare quark masses. (Of course the value of the expansion parameters will be different, but the structure of the expansion will be the same. We shall discuss this point a little further in section 2.4.)

So in the following we need not usually distinguish between bare and renormalised quark masses.

Note that

$$\delta m_u + \delta m_d + \delta m_s = 0\,, \tag{11}$$

so we could eliminate one of these symbols. However we shall keep all three symbols as we can then write some expressions in a more obviously symmetrical form.

2.2 General strategy

With this notation, the quark mass matrix is

$$\begin{aligned}
\mathcal{M} &= \begin{pmatrix} m_u & 0 & 0 \\ 0 & m_d & 0 \\ 0 & 0 & m_s \end{pmatrix} \\
&= \overline{m} \begin{pmatrix} 1 & 0 & 0 \\ 0 & 1 & 0 \\ 0 & 0 & 1 \end{pmatrix} \\
&\quad + \tfrac{1}{2}(\delta m_u - \delta m_d) \begin{pmatrix} 1 & 0 & 0 \\ 0 & -1 & 0 \\ 0 & 0 & 0 \end{pmatrix} + \tfrac{1}{2}\delta m_s \begin{pmatrix} -1 & 0 & 0 \\ 0 & -1 & 0 \\ 0 & 0 & 2 \end{pmatrix} .
\end{aligned} \tag{12}$$

The mass matrix $\mathcal{M}$ has a singlet part (proportional to I) and an octet part, proportional to λ_3, λ_8. We argue here that the theoretically cleanest way to approach the physical point is to keep the singlet part of $\mathcal{M}$ constant, and vary only the non-singlet parts.

An important advantage of our strategy is that it strongly constrains the possible mass dependence of physical quantities, and so simplifies the extrapolation towards the physical point. Consider a flavour singlet quantity, which we shall denote by X_S, at the symmetric point (m_0, m_0, m_0). Examples are the scale[2] $X_r = r_0^{-1}$, or the plaquette P (this will soon be generalised to other singlet quantities). If we make small changes in the quark masses, symmetry requires that the derivatives at the symmetric point are equal

$$\frac{\partial X_r}{\partial m_u} = \frac{\partial X_r}{\partial m_d} = \frac{\partial X_r}{\partial m_s}\,. \tag{13}$$

[2]There is no significance here to using r_0 or r_0^{-1}; however defining $X_r = r_0^{-1}$ is more consistent with later definitions.

If we keep $m_u + m_d + m_s$ constant, $\delta m_s = -\delta m_u - \delta m_d$ so

$$\delta X_r = \frac{\partial X_r}{\partial m_u}\delta m_u + \frac{\partial X_r}{\partial m_d}\delta m_d + \frac{\partial X_r}{\partial m_s}\delta m_s = 0\,. \tag{14}$$

The effect of making the strange quark heavier exactly cancels the effect of making the light quarks lighter, so we know that X_r must be stationary at the symmetrical point. This makes extrapolations towards the physical point much easier, especially since we find that in practice quadratic terms in the quark mass expansion are very small. Any permutation of the quarks, such as an interchange $u \leftrightarrow s$, or a cyclic permutation $u \to d \to s \to u$ doesn't change the physics, it just renames the quarks. Any quantity unchanged by all permutations will be flat at the symmetric point, like X_r.

We can also construct permutation-symmetric combinations of hadrons. For orientation in Fig. 2 we give the octet multiplets for spin 0 (pseudoscalar) and

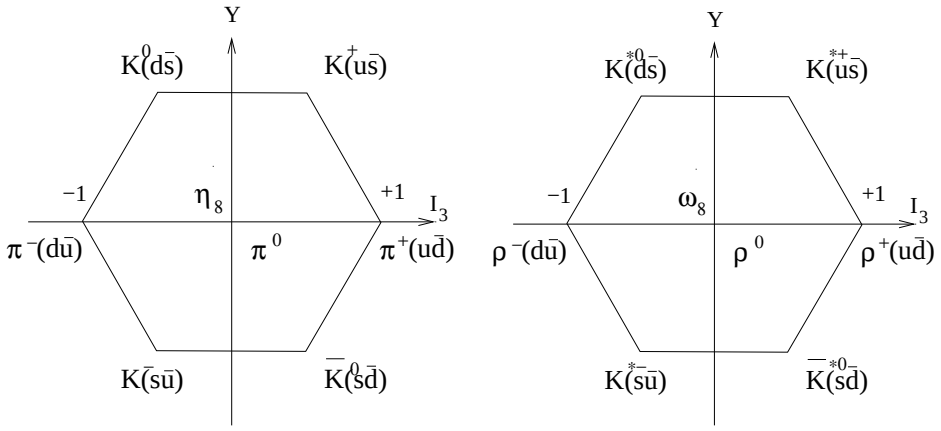

Figure 2: The octets for spin 0 (pseudoscalar) and spin 1 (vector) mesons.

spin 1 (vector) mesons and in Fig. 3 the lowest octet and decuplet multiplets for the spin $\frac{1}{2}$ and for the $\frac{3}{2}$ baryons (all plotted in the I_3–Y plane).

For example, for the decuplet, any permutation of the quark labels will leave the $\Sigma^{*0}(uds)$ unchanged, so the Σ^{*0} is shown by a single black point in Fig. 4. On the other hand, a permutation (such as $u \to d \to s$) can change a $\Delta^{++}(uuu)$ into a $\Delta^{-}(ddd)$ or (if repeated) into an $\Omega^{-}(sss)$, so these three particles form a set of baryons which is closed under quark permutations, and are all given the same colour (red) in Fig. 4. Finally the 6 baryons consisting of two quarks of one flavour, and one quark of a different flavour, form an invariant set, shown in blue in Fig. 4.

If we sum the masses in any of these sets, we get a flavour symmetric quantity, which will obey the same argument we gave in eq. (14) for the quark mass (in)dependence of the scale r_0. We therefore expect that the Σ^{0*} mass

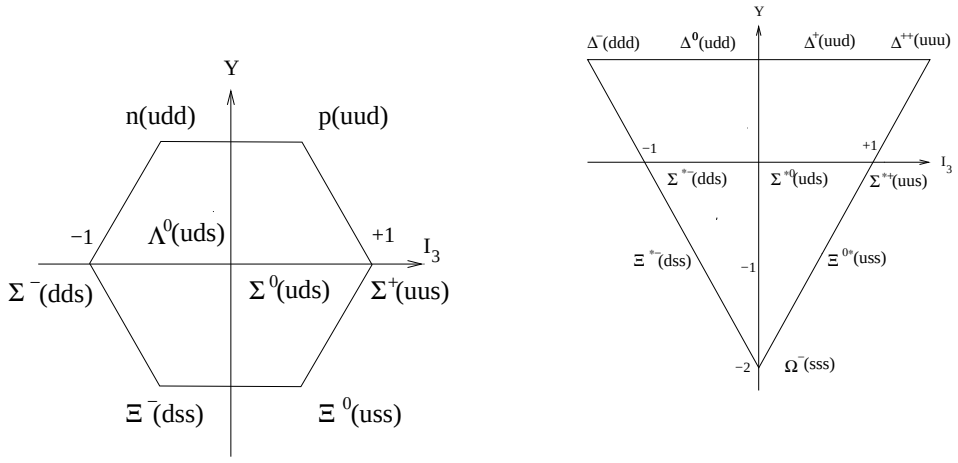

Figure 3: The lowest octet and decuplets for the spin $\frac{1}{2}$ and for the $\frac{3}{2}$ baryons (plotted in the I_3–Y plane.

must be flat at the symmetric point, and furthermore that the combinations $(M_{\Delta^{++}} + M_{\Delta^-} + M_\Omega)$ and $(M_{\Delta^+} + M_{\Delta^0} + M_{\Sigma^{*+}} + M_{\Sigma^{*-}} + M_{\Xi^{*0}} + M_{\Xi^{*-}})$ will also be flat. Technically these symmetrical combinations are in the A_1 singlet representation of the permutation group S_3. This is the symmetry group of an equilateral triangle, C_{3v}. This group has 3 irreducible representations, [6], two different singlets, A_1 and A_2 and a doublet E, with elements E^+, E^-. Some details of this group and its representations are given in Appendix A, while Table 1 gives a summary of the transformations.

	A_1	E		A_2
Op		E^+	E^-	
Identity	+	+	+	+
$u \leftrightarrow d$	+	+	−	−
$u \leftrightarrow s$	+	mix		−
$d \leftrightarrow s$	+	mix		−
$u \to d \to s \to u$	+	mix		+
$u \to s \to d \to u$	+	mix		+

Table 1: A simplified table showing how the group operations of S_3 act in the different representations: + refers to unchanged; − to reflection.

We list some of these invariant mass combinations in Table 2. The permutation group S_3 yields a lot of useful relationships, but cannot capture the entire structure. For example, there is no way to make a connection between the

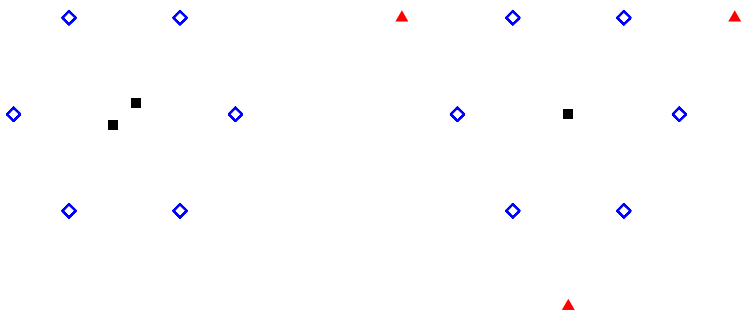

Figure 4: The behaviour of the octet and decuplet under the permutation group S_3. The colours denote sets of particles which are invariant under permutations of the quark flavours (red or filled triangles, blue or open diamonds and black or filled squares).

Pseudoscalar	$X_\pi^2 = \frac{1}{6}(M_{K^+}^2 + M_{K^0}^2 + M_{\pi^+}^2 + M_{\pi^-}^2 + M_{\overline{K}^0}^2 + M_{K^-}^2)$	blue
mesons	$X_{\eta_8}^2 = \frac{1}{2}(M_{\pi^0}^2 + M_{\eta_8}^2)$	black
Vector	$X_\rho = \frac{1}{6}(M_{K^{*+}} + M_{K^{*0}} + M_{\rho^+} + M_{\rho^-} + M_{\overline{K}^{*0}} + M_{K^{*-}})$	blue
mesons	$X_{\phi_s} = \frac{1}{3}(2M_{\rho^0} + M_{\phi_s})$	black
Octet	$X_N = \frac{1}{6}(M_p + M_n + M_{\Sigma^+} + M_{\Sigma^-} + M_{\Xi^0} + M_{\Xi^-})$	blue
baryons	$X_\Lambda = \frac{1}{2}(M_{\Lambda^0} + M_{\Sigma^0})$	black
Decuplet	$X_\Delta = \frac{1}{3}(M_{\Delta^{++}} + M_{\Delta^-} + M_{\Omega^-})$	red
baryons	$X_{\Xi^*} = \frac{1}{6}(M_{\Delta^+} + M_{\Delta^0} + M_{\Sigma^{*+}} + M_{\Sigma^{*-}} + M_{\Xi^{*0}} + M_{\Xi^{*-}})$	blue
	$X_{\Sigma^*} = M_{\Sigma^{*0}}$	black

Table 2: Permutation invariant mass combinations, see Fig. 4. ϕ_s is a fictitious $s\overline{s}$ particle; η_8 a pure octet meson. The colours in the third column correspond to Fig. 4.

$\Delta^{++}(uuu)$ and the $\Delta^+(uud)$ by permuting quarks. To go further, we need to classify physical quantities by $SU(3)$ (containing the permutation group S_3 as a subgroup), which we shall now consider.

2.3 Taylor expansion

We will Taylor expand about a symmetric reference point

$$(m_u, m_d, m_s) = (m_0, m_0, m_0)\,. \tag{15}$$

Our results will be polynomials in the quark masses, we will express them in terms of the δm_q of eq. (9). The main idea is to classify all possible mass polynomials by their transformation properties under the permutation group S_3 and under the full flavour group $SU(3)$, and classify hadronic observables the same way. The Taylor expansion of a given observable can only include the polynomials of

the same symmetry. The Taylor expansions of hadronic quantities in the same $SU(3)$ multiplet but in different S_3 representations will have related expansion coefficients.

We can always arrange polynomials to be in definite permutation group states. When we get to polynomials of $O(\delta m_q^2)$ we find that a polynomial may be a mixture of several $SU(3)$ representations, but the classification is still useful. In Table 3 we classify all the polynomials which could occur in a Taylor expansion

Polynomial		S_3	$SU(3)$					
1	✓	A_1	1					
$(\overline{m}-m_0)$		A_1	1					
δm_s	✓	E^+		8				
$(\delta m_u-\delta m_d)$	✓	E^-		8				
$(\overline{m}-m_0)^2$		A_1	1					
$(\overline{m}-m_0)\delta m_s$		E^+		8				
$(\overline{m}-m_0)(\delta m_u-\delta m_d)$		E^-		8				
$\delta m_u^2+\delta m_d^2+\delta m_s^2$	✓	A_1	1				27	
$3\delta m_s^2-(\delta m_u-\delta m_d)^2$	✓	E^+		8			27	
$\delta m_s(\delta m_d-\delta m_u)$	✓	E^-		8			27	
$(\overline{m}-m_0)^3$		A_1	1					
$(\overline{m}-m_0)^2\delta m_s$		E^+		8				
$(\overline{m}-m_0)^2(\delta m_u-\delta m_d)$		E^-		8				
$(\overline{m}-m_0)(\delta m_u^2+\delta m_d^2+\delta m_s^2)$		A_1	1				27	
$(\overline{m}-m_0)\left[3\delta m_s^2-(\delta m_u-\delta m_d)^2\right]$		E^+		8			27	
$(\overline{m}-m_0)\delta m_s(\delta m_d-\delta m_u)$		E^-		8			27	
$\delta m_u\delta m_d\delta m_s$	✓	A_1	1				27	64
$\delta m_s(\delta m_u^2+\delta m_d^2+\delta m_s^2)$	✓	E^+		8			27	64
$(\delta m_u-\delta m_d)(\delta m_u^2+\delta m_d^2+\delta m_s^2)$	✓	E^-		8			27	64
$(\delta m_s-\delta m_u)(\delta m_s-\delta m_d)(\delta m_u-\delta m_d)$	✓	A_2			10	$\overline{10}$		64

Table 3: All the quark-mass polynomials up to $O(m_q^3)$, classified by symmetry properties. A tick (✓) marks the polynomials relevant on a constant $\overline{m}$ surface. These polynomials are plotted in Fig. 6.

about the symmetric point, eq. (15), up to $O(\delta m_q^3)$. Many of the polynomials in the table have factors of $(\overline{m}-m_0)$, these polynomials drop out if we restrict ourselves to the surface of constant $\overline{m}=m_0$, leaving only the polynomials marked with a tick (✓) in Table 3.

Since we are keeping $\overline{m}$ constant, we are only changing the octet part of the mass matrix in eq. (12). Therefore, to first order in the mass change, only octet quantities can be affected. $SU(3)$ singlets have no linear dependence on the quark mass, as we have already seen by the symmetry argument eq. (14), but we now

see that all quantities in $SU(3)$ multiplets higher than the octet cannot have linear terms. This provides a constraint on the hadron masses within a multiplet and leads (as we shall see) to the Gell-Mann Okubo mass relations [10, 11].

When we proceed to quadratic polynomials we can construct polynomials which transform like mixtures of the 1, 8 and 27 multiplets of $SU(3)$, Table 3. This covers all the structures that can arise in the octet mass matrix, but the decuplet mass matrix can include terms with the symmetries 10, $\overline{10}$, and 64, which first occur when we look at cubic polynomials in the quark masses, Table 3.

In a little more detail constructing polynomials with a definite S_3 classification is fairly straightforward, we simply have to see what happens to each polynomial under simple interchanges (e.g. $u \leftrightarrow d$) and cyclic permutations (e.g. $u \to s$, $s \to d$, $d \to u$). The S_3 column of Table 3 is easy to check by hand. The $SU(3)$ assignment of polynomials is less straightforward. Only the simplest polynomials belong purely to a single $SU(3)$ multiplet; most polynomials contain mixtures of several multiplets. The non-singlet mass is an octet of $SU(3)$, so quadratic polynomials in δm_q can contain representations which occur in $8 \otimes 8$, cubic polynomials representations which occur in $8 \otimes 8 \otimes 8$. We can find out what representations are present in a given polynomial by using the Casimir operators of $SU(3)$ [12, 13]. That operator was programmed in Mathematica, and used to analyse our polynomial basis. Some more details are presented in Appendix B.2. The results of the calculation are recorded in the $SU(3)$ section of Table 3.

The allowed quark mass region on the $\overline{m} = $ const. surface is an equilateral triangle, as shown in Fig. 5. Plotting the polynomials of Table 3 then gives the plots in Fig. 6, where the colour coding indicates whether the polynomial is positive (red) or negative (blue). As a first example of the use of these tables, consider the Taylor expansion for the scale r_0/a. As discussed previously, this is a gluonic quantity, blind to flavour, so it has symmetry A_1 under the S_3 permutation group. Therefore its Taylor expansion only contains polynomials of symmetry A_1. If we keep $\overline{m}$, the average quark mass, fixed, the expansion of r_0/a must take the form

$$\frac{r_0}{a} = \alpha + \beta(\delta m_u^2 + \delta m_d^2 + \delta m_s^2) + \gamma\, \delta m_u \delta m_d \delta m_s + \dots \,, \tag{16}$$

with just 3 coefficients. Interestingly, we could find all 3 coefficients from $2 + 1$ data, so we would be able to predict $1 + 1 + 1$ flavour results from fits to $2 + 1$ data. This is common. If we are not on a constant $\overline{m}$ surface, we would need 7 coefficients to give a cubic fit for r_0; if we did not have any information on the symmetry of r_0 we would need 20 coefficients. If we additionally use r_0 data from the equal mass calculations we also have a good estimate of the coefficient of $(\overline{m} - m_0)$, which we can use to estimate the effect of shifting from one value of $\overline{m}$ to another.

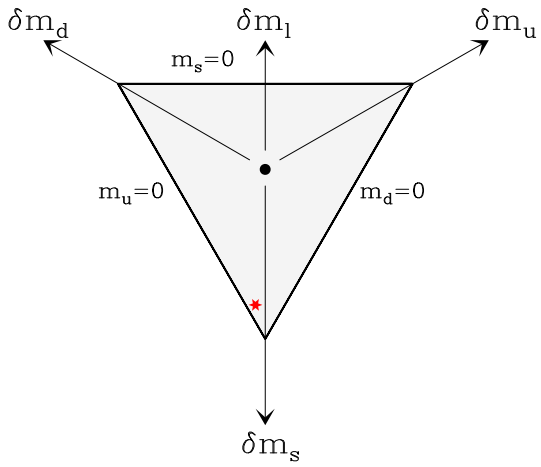

Figure 5: The allowed quark mass region on the $\overline{m} = \text{const.}$ surface is an equilateral triangle. The black point at the center is the symmetric point, the red star is the physical point. $2+1$ simulations lie on the vertical symmetry axis. The physical point is slightly off the $2+1$ axis because $m_d > m_u$.

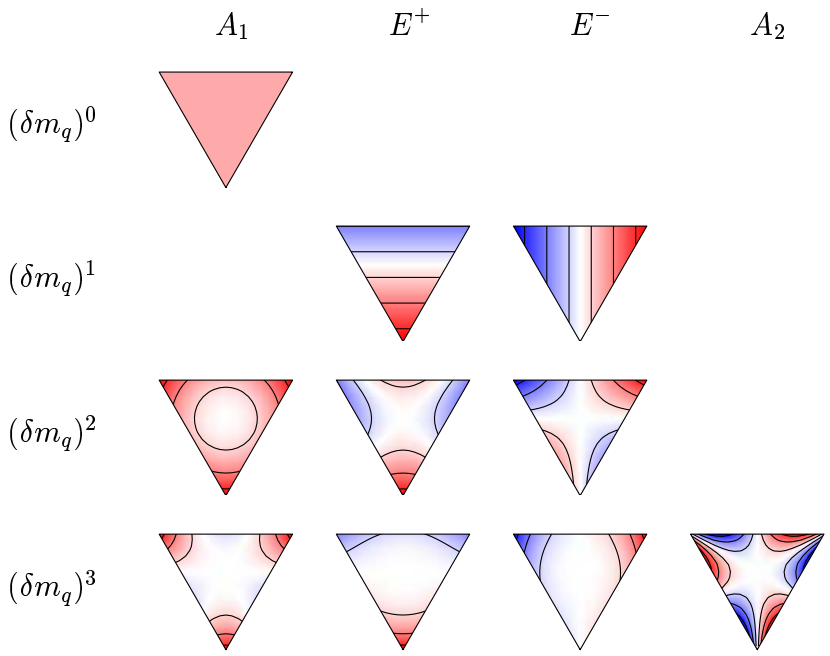

Figure 6: Contour plots of the polynomials relevant for the constant $\overline{m}$ Taylor expansion, see Table 3. A red(dish) colour denotes a positive number while a blue(ish) colour indicates a negative number. If $m_u = m_d$ (the $2+1$ case), only the polynomials in the A_1 and E^+ columns contribute.

2.4 O(a)-improvement of quark masses

Before classifying the hadron mass matrix, we pause and consider the $O(a)$ improvement of quark masses. (If we are considering chiral fermions, we have 'automatic $O(a)$ improvement', see eg [7] for a discussion.) In writing down expressions for bare and improved quark masses, it is natural to expand about the chiral point, all three quarks massless, which means setting $m_0 = 0$ in the expressions in Table 3. Later, when we consider lattice results, we want our expansion point to be a point where we can run simulations, so we will normally have a non-zero m_0.

Improving the quark masses requires us to add improvement terms of the type am_q^2 to the bare mass. We can add $SU(3)$-singlet improvement terms to the singlet quark mass, $SU(3)$-octet improvement terms to the non-singlet quark mass. We are led to the following expressions for the improved and renormalised quark masses

$$\begin{aligned} \overline{m}^R &= Z_m^S \left[\overline{m} + a\left\{b_1\overline{m}^2 + b_2(\delta m_s^2 + \delta m_u^2 + \delta m_d^2)\right\}\right] \\ \delta m_s^R &= Z_m^{NS} \left[\delta m_s + a\left\{b_3\overline{m}\delta m_s + b_4(3\delta m_s^2 - (\delta m_u - \delta m_d)^2)\right\}\right] , \end{aligned} \tag{17}$$

together with $Z_m^S = Z_m^{NS} r_m$, eqs. (5), (6). We have improved $\overline{m}$ by adding the two possible singlet terms from the quadratic section of Table 3, and improved δm_s by adding the two possible E^+ octet polynomials. These 4 improvement terms match the 4 terms introduced in [8][3]. We get expressions for the u and d quark mass improvement by flavour-permuting eq. (17)

$$\begin{aligned} \delta m_u^R &= Z_m^{NS} \left[\delta m_u + a\left\{b_3\overline{m}\delta m_u + b_4(3\delta m_u^2 - (\delta m_d - \delta m_u)^2)\right\}\right] \\ \delta m_d^R &= Z_m^{NS} \left[\delta m_d + a\left\{b_3\overline{m}\delta m_d + b_4(3\delta m_d^2 - (\delta m_s - \delta m_d)^2)\right\}\right] \\ \delta m_u^R - \delta m_d^R &= Z_m^{NS} \left[\delta m_u - \delta m_d + a\left\{b_3\overline{m}(\delta m_u - \delta m_d) + 6b_4\delta m_s(\delta m_d - \delta m_u)\right\}\right] . \end{aligned} \tag{18}$$

The improvement terms for $\delta m_u - \delta m_d$ are proportional to the two E^-, $SU(3)$-

[3] Ref. [8] gives the $O(a)$ improved quark mass as

$$\begin{aligned} m_q^R &= Z_m^{NS} \Big[m_q + (r_m - 1)\overline{m} \\ &\quad + a\left\{b_m m_q^2 + 3\overline{b}_m m_q\overline{m} + (r_m d_m - b_m)\overline{m^2} + 3(r_m\overline{d}_m - \overline{b}_m)\overline{m}^2\right\}\Big] , \end{aligned}$$

where $\overline{m^2} = \frac{1}{3}(m_u^2 + m_d^2 + m_s^2)$. This is an expansion around the chiral point ($m_q = 0$) while we have an expansion about a flavour symmetric point, m_0 ($m_0 = 0$ here). So we have to match the expansions, which gives the results

$$\begin{array}{rcl} b_m &=& 6b_4 \\ \overline{b}_m &=& \frac{1}{3}b_3 - 4b_4 \\ d_m &=& 3b_2 \\ \overline{d}_m &=& \frac{1}{3}b_1 - b_2 \end{array} , \quad \text{or} \quad \begin{array}{rcl} b_1 &=& 3\overline{d}_m + d_m \\ b_2 &=& \frac{1}{3}d_m \\ b_3 &=& 3\overline{b}_m + 2b_m \\ b_4 &=& \frac{1}{6}b_m \end{array} .$$

octet, quadratic polynomials[4].

Table 3 is based purely on flavour arguments, we would hope that all the results are true whether we use bare or renormalised quantities, and also independently of whether we work with a naive bare mass, or a bare mass with $O(a)$ improvement terms. Let us check if this is true. The first thing we need to know is whether the zero-sum identity eq. (11) survives renormalisation and improvement. Using the previous equations we find

$$\begin{aligned} \delta m_u^R + \delta m_d^R + \delta m_s^R &= Z_m^{NS}\left[(\delta m_u + \delta m_d + \delta m_s) + b_3 a\overline{m}(\delta m_u + \delta m_d + \delta m_s)\right. \\ &\qquad \left. + b_4 a(\delta m_u + \delta m_d + \delta m_s)^2\right] \\ &= 0\,, \end{aligned} \tag{19}$$

showing that eq. (11) is not violated by improvement or renormalisation.

The next point we want to check is whether the symmetry of a polynomial depends on whether we expand in terms of improved masses or unimproved. As an example, let us look at the quadratic polynomial

$$\delta m_s^R(\delta m_d^R - \delta m_u^R)\,, \tag{20}$$

which has permutation symmetry E^-, and $SU(3)$ content octet and 27-plet. Expanding to first order in lattice spacing a we find

$$\begin{aligned} \delta m_s^R(\delta m_d^R - \delta m_u^R) &= (Z_m^{NS})^2\left[\delta m_s(\delta m_d - \delta m_u)\right. \\ &\qquad + a\left(2b_3\overline{m}\delta m_s(\delta m_d - \delta m_u)\right. \\ &\qquad \left.\left. + \,2b_4(\delta m_u - \delta m_d)(\delta m_u^2 + \delta m_d^2 + \delta m_s^2)\right)\right]\,. \end{aligned} \tag{21}$$

The mass improvement terms have generated two extra cubic polynomials, but they are both polynomials with the same symmetry as the initial polynomial, showing that Table 3 applies both to improved and unimproved masses.

Thus our conclusion is that the flavour expansion results are true whether we use bare or renormalised quantities, and also independently of whether we work with a naive bare mass, or a bare mass with $O(a)$ improvement terms.

2.5 SU(3) and S_3 classification of hadron mass matrices

In eq. (12) we split the quark mass matrix into a singlet part and two octet parts. We want to make a similar decomposition of the hadron mass matrices. We start with the decuplet mass matrix because it is simpler than the octet mass matrix.

[4]We have to use the identity, eq. (11), to bring the result to the desired form – which will often be the case in what follows.

2.5.1 The decuplet mass matrix

The decuplet mass matrix is a 10×10 diagonal matrix. From $SU(3)$ group algebra we know

$$10 \otimes \overline{10} = 1 \oplus 8 \oplus 27 \oplus 64\,. \tag{22}$$

The singlet matrix is the identity matrix, the octet representation contains 2 diagonal matrices (λ_3 and λ_8), the 27-plet has 3 diagonal matrices, and the 64-plet includes 4 diagonal matrices, see Fig. 7. This gives us a basis of 10 diagonal

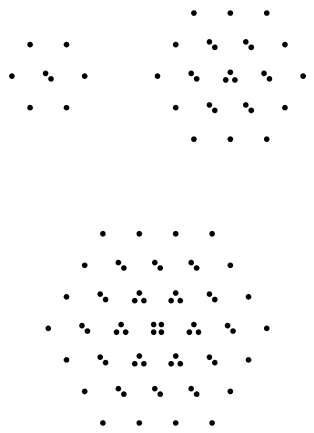

Figure 7: The octet, 27-plet and 64-plet representations of $SU(3)$. The number of spots in the central location gives the number of flavour-conserving operators in each multiplet. In the octet, the 2 operators form an E doublet of the permutation group. In the 27-plet the 3 operators are an A_1 singlet and an E doublet. In the 64-plet the centre operators are an A_1 singlet, an E doublet and an A_2 singlet.

matrices, into which we can decompose the decuplet mass matrix.

We can use the Casimir operator to project out the diagonal matrices in a particular $SU(3)$ representation. We find, for example, that the octet matrix with S_3 symmetry E^- is:

$$\begin{array}{c} \Delta^- \;\; \Delta^0 \;\; \Delta^+ \;\; \Delta^{++} \; \Sigma^{*-} \;\; \Sigma^{*0} \;\; \Sigma^{*+} \;\; \Xi^{*-} \;\; \Xi^{*0} \;\; \Omega^- \\ \left(\begin{array}{cccccccccc} -3 & 0 & 0 & 0 & 0 & 0 & 0 & 0 & 0 & 0 \\ 0 & -1 & 0 & 0 & 0 & 0 & 0 & 0 & 0 & 0 \\ 0 & 0 & 1 & 0 & 0 & 0 & 0 & 0 & 0 & 0 \\ 0 & 0 & 0 & 3 & 0 & 0 & 0 & 0 & 0 & 0 \\ 0 & 0 & 0 & 0 & -2 & 0 & 0 & 0 & 0 & 0 \\ 0 & 0 & 0 & 0 & 0 & 0 & 0 & 0 & 0 & 0 \\ 0 & 0 & 0 & 0 & 0 & 0 & 2 & 0 & 0 & 0 \\ 0 & 0 & 0 & 0 & 0 & 0 & 0 & -1 & 0 & 0 \\ 0 & 0 & 0 & 0 & 0 & 0 & 0 & 0 & 1 & 0 \\ 0 & 0 & 0 & 0 & 0 & 0 & 0 & 0 & 0 & 0 \end{array}\right) \end{array} \equiv \begin{array}{ccccccc} & & -3 & & -1 & & 1 & & 3 \\ & & & -2 & & 0 & & 2 & \\ & & & & -1 & & 1 & & \\ & & & & & 0 & & & \end{array} \tag{23}$$

where we have used a more compact notation to record the diagonal elements on the right-hand side. The entry in the Δ^- column of the matrix is -3, so on the right-hand side we put a -3 in the position of the Δ^- in the usual decuplet diagram, and so on. In Fig. 8 we show all 10 diagonal matrices, in this compact

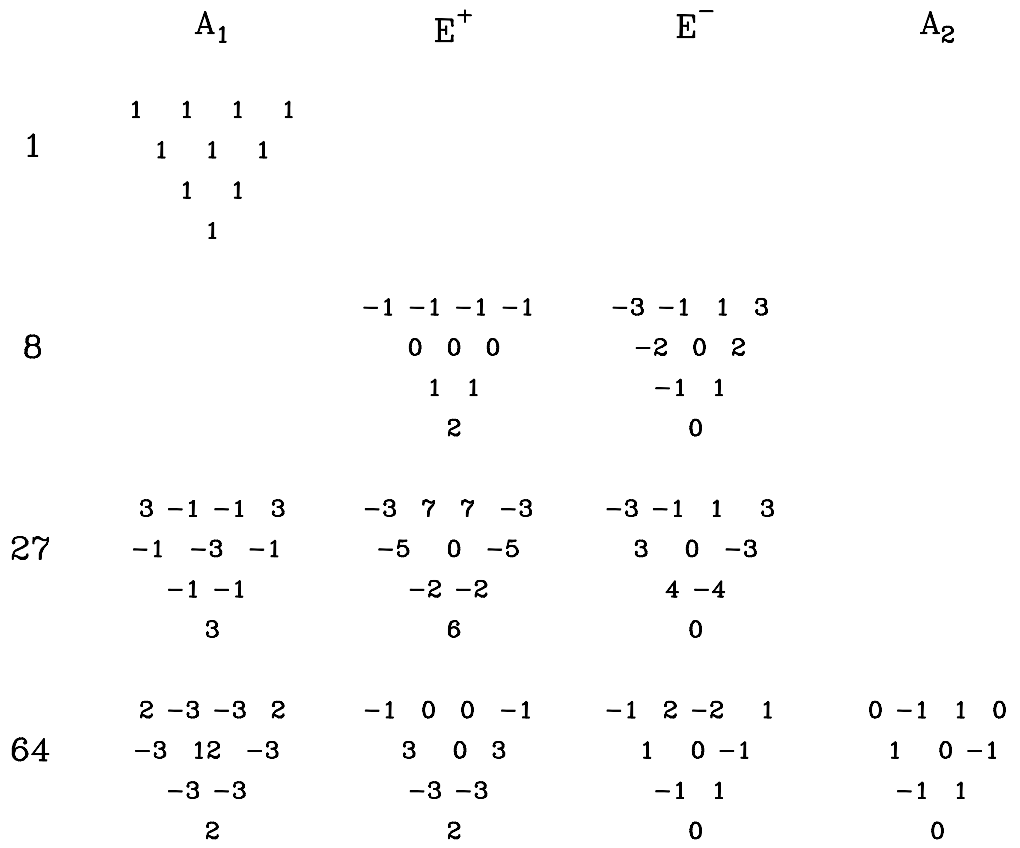

Figure 8: The matrices for projecting out decuplet mass contributions of known symmetry – see eq. (23) for an explanation of the notation.

notation. These matrices are orthogonal, in the sense

$$\mathrm{Tr}[\tau_a \tau_b] = 0 \quad \text{if} \quad a \neq b\,, \tag{24}$$

so they can be used to project out mass combinations which have simple quark mass dependencies, see Fig. 8, and Table 4. As an example of a mass formula we look at the singlet of the decuplet mass matrix. This gives from Table 4,

$$\begin{aligned} & M_{\Delta^-} + M_{\Delta^0} + M_{\Delta^+} + M_{\Delta^{++}} \\ & + M_{\Sigma^{*-}} + M_{\Sigma^{*0}} + M_{\Sigma^{*+}} + M_{\Xi^{*-}} + M_{\Xi^{*0}} + M_{\Omega^-} \\ & \quad = \; 10 M_0 \; + B_1 \left(\delta m_u^2 + \delta m_d^2 + \delta m_s^2\right) + C_1 \, \delta m_u \delta m_d \delta m_s + \ldots \,. \end{aligned} \tag{25}$$

As a further example for the 27-plet component of the decuplet mass matrix, we see from Table 4 that there are three mass combinations which transform as

Δ^-	Δ^0	Δ^+	Δ^{++}	Σ^{*-}	Σ^{*0}	Σ^{*+}	Ξ^{*-}	Ξ^{*0}	Ω^-	S_3	$SU(3)$
1	1	1	1	1	1	1	1	1	1	A_1	1
−1	−1	−1	−1	0	0	0	1	1	2	E^+	8
−3	−1	1	3	−2	0	2	−1	1	0	E^-	8
3	−1	−1	3	−1	−3	−1	−1	−1	3	A_1	27
−3	7	7	−3	−5	0	−5	−2	−2	6	E^+	27
−3	−1	1	3	3	0	−3	4	−4	0	E^-	27
2	−3	−3	2	−3	12	−3	−3	−3	2	A_1	64
−1	0	0	−1	3	0	3	−3	−3	2	E^+	64
−1	2	−2	1	1	0	−1	−1	1	0	E^-	64
0	−1	1	0	1	0	−1	−1	1	0	A_2	64

Table 4: Decuplet mass matrix contributions, classified by permutation and $SU(3)$ symmetry, see Fig. 8.

27-plets, giving three related mass relations

$$
\begin{aligned}
&3M_{\Delta^-} - M_{\Delta^0} - M_{\Delta^+} + 3M_{\Delta^{++}} \\
&-M_{\Sigma^{*-}} - 3M_{\Sigma^{*0}} - M_{\Sigma^{*+}} - M_{\Xi^{*-}} - M_{\Xi^{*0}} + 3M_{\Omega^-} \\
&\quad = b_{27}\left[\delta m_u^2 + \delta m_d^2 + \delta m_s^2\right] + 9c_{27}\delta m_u \delta m_d \delta m_s + \ldots \\
&-3M_{\Delta^-} + 7M_{\Delta^0} + 7M_{\Delta^+} - 3M_{\Delta^{++}} \\
&-5M_{\Sigma^{*-}} - 5M_{\Sigma^{*+}} - 2M_{\Xi^{*-}} - 2M_{\Xi^{*0}} + 6M_{\Omega^-} \\
&\quad = b_{27}\left[3\delta m_s^2 - (\delta m_u - \delta m_d)^2\right] + 3c_{27}\delta m_s\left(\delta m_u^2 + \delta m_d^2 + \delta m_s^2\right) + \ldots \\
&-3M_{\Delta^-} - M_{\Delta^0} + M_{\Delta^+} + 3M_{\Delta^{++}} \\
&+3M_{\Sigma^{*-}} - 3M_{\Sigma^{*+}} + 4M_{\Xi^{*-}} - 4M_{\Xi^{*0}} \\
&\quad = 2b_{27}(\delta m_d - \delta m_u)\delta m_s + c_{27}(\delta m_u - \delta m_d)\left(\delta m_u^2 + \delta m_d^2 + \delta m_s^2\right) + \ldots
\end{aligned}
\tag{26}
$$

Note that we can find all the coefficients in these equations from a 2+1 simulation, and use them to (fully) predict the results of a $1+1+1$ simulation.

2.5.2 The octet mass matrix

We can analyse the possible terms in the octet mass matrix in the same way as we did for the decuplet. However there is a complication in the octet case which we do not have in the decuplet, caused by the fact that we have two particles (the Λ and Σ^0) with the same Y and I_3 quantum numbers. If $m_u \neq m_d$ these states mix. There are interesting connections between the elements of the Λ/Σ^0 mixing matrix and the splittings of the other baryons, but since in this article we are concerned with $2+1$ simulations, where this mixing does not arise, we will not discuss this further here.

We can however pick out several useful mass relations which are unaffected by Λ/Σ^0 mixing.

$$\begin{aligned} & M_n + M_p + M_\Lambda + M_{\Sigma^-} + M_{\Sigma^0} + M_{\Sigma^+} + M_{\Xi^-} + M_{\Xi^0} \\ & \quad = \; 8M_0 + b_1(\delta m_u^2 + \delta m_d^2 + \delta m_s^2) + c_1 \delta m_u \delta m_d \delta m_s + \dots \, . \\ & M_n + M_p - 3M_\Lambda + M_{\Sigma^-} - 3M_{\Sigma^0} + M_{\Sigma^+} + M_{\Xi^-} + M_{\Xi^0} \\ & \quad = \; b_{27}(\delta m_u^2 + \delta m_d^2 + \delta m_s^2) \, . \end{aligned} \tag{27}$$

At order δm_q^3 we meet some quantities in the baryon octet masses (the 10 and $\overline{10}$ combinations) which can not be deduced from $2+1$ flavour measurements – though valence $1+1+1$ on a $2+1$ background would be a possible method of estimating these quantities. (We also do not pursue this further here.)

2.6 The Coleman-Glashow mass relation

One early prediction concerning hyperon masses was the Coleman-Glashow relation [9]

$$M_n - M_p - M_{\Sigma^-} + M_{\Sigma^+} + M_{\Xi^-} - M_{\Xi^0} \approx 0 \, . \tag{28}$$

Deviations from this relation are barely detectable. This mass combination appear in Table 5 as one of the A_2 quantities. We can understand the success of the

n	p	Σ^-	Σ^0	Λ	Σ^+	Ξ^-	Ξ^0	S_3	$SU(3)$
1	1	1	1	1	1	1	1	A_1	1
-1	-1	0	0	0	0	1	1	E^+	8_a
-1	1	-2	0	0	2	-1	1	E^-	8_a
1	1	-2	-2	2	-2	1	1	E^+	8_b
-1	1	0	mix		0	1	-1	E^-	8_b
1	1	1	-3	-3	1	1	1	A_1	27
1	1	-2	3	-3	-2	1	1	E^+	27
-1	1	0	mix		0	1	-1	E^-	27
1	-1	-1	0	0	1	1	-1	A_2	$10,\overline{10}$
0	0	0	mix		0	0	0	A_2	$10,\overline{10}$

Table 5: Mass matrix contributions for octet baryons, classified by permutation and $SU(3)$ symmetry. Note that the first two octet quantities (the 8_a) are proportional to the hypercharge Y and to isospin I_3 respectively.

Coleman-Glashow relation by noting that the only polynomial in Table 3 with A_2 symmetry is $O(\delta m_q^3)$, so that the predicted violation of the Coleman-Glashow relation is

$$\begin{aligned} & M_n - M_p - M_{\Sigma^-} + M_{\Sigma^+} + M_{\Xi^-} - M_{\Xi^0} \\ & \quad = \; c_{10}(\delta m_s - \delta m_u)(\delta m_s - \delta m_d)(\delta m_u - \delta m_d) \, . \end{aligned} \tag{29}$$

The polynomial is zero if any pair of quarks have the same mass, so we would need to measure the masses of baryons in a $1+1+1$ setting to determine c_{10} and predict the violation of the Coleman-Glashow relation.

3 Theory: $2+1$ flavours

If we take any mass relation from the $1+1+1$ section, and put $m_u = m_d = m_l$ we will get a valid mass relation for the $2+1$ case. In the $2+1$ case only one parameter is needed to measure the symmetry breaking, because of eq. (11),

$$\delta m_s = -2\delta m_l \,, \tag{30}$$

where

$$\delta m_l = m_l - m_0 \,. \tag{31}$$

In the $2+1$ limit the decuplet baryons have 4 different masses (for the Δ, Σ^*, Ξ^*, and Ω). Similarly, for the octet baryons there are also 4 distinct masses, $(N, \Lambda, \Sigma, \Xi)$; and for octet mesons, 3 masses. In the meson octet the K and $\overline{K}$ must have the same mass, but there is no reason why the N and Ξ (which occupy the corresponding places in the baryon octet), should have equal masses once flavour $SU(3)$ is broken.

Again we have the singlet quantities X_S which are stationary at the symmetry point as given in Table 2, but which now simplify to give Table 6. In the notation

Pseudoscalar	$X_\pi^2 = \frac{1}{3}(2M_K^2 + M_\pi^2)$	blue
mesons	$X_{\eta_8}^2 = \frac{1}{2}(M_\pi^2 + M_{\eta_8}^2)$	black
Vector	$X_\rho = \frac{1}{3}(2M_{K^*} + M_\rho)$	blue
mesons	$X_{\phi_s} = \frac{1}{3}(2M_\rho + M_{\phi_s})$	black
Octet	$X_N = \frac{1}{3}(M_N + M_\Sigma + M_\Xi)$	blue
baryons	$X_\Lambda = \frac{1}{2}(M_\Sigma + M_\Lambda)$	black
Decuplet	$X_\Delta = \frac{1}{3}(2M_\Delta + M_\Omega)$	red
baryons	$X_{\Xi^*} = \frac{1}{3}(M_\Delta + M_{\Sigma^*} + M_{\Xi^*})$	blue
	$X_{\Sigma^*} = M_{\Sigma^*}$	black

Table 6: Permutation invariant mass combinations, see Fig. 4. ϕ_s is a fictitious $s\overline{s}$ particle; η_8 a pure octet meson. The colours in the third column correspond to Fig. 4.

we have now assumed isospin invariance, so that for example $M_\Delta \equiv M_{\Delta^{++}} = M_{\Delta^-} = M_{\Delta^+} = M_{\Delta^0}$. (The corresponding mass values we use in this article are given in section 9.)

Furthermore this can obviously be generalised. Let us first define $m_\eta = (m_l + 2m_s)/3$ and $m_K = (m_l + m_s)/2$. Then $m_l + m_\eta = 2\overline{m}$ and $m_l + 2m_K = 3\overline{m}$ are

constants on our trajectory and so $\delta m_l + \delta m_\eta = 0$ and also $\delta m_l + 2\delta m_K = 0$. For example, this means that any functions of the form

$$2f(m_K) + f(m_l) \quad \text{or} \quad g(m_s) + 2g(m_l) \quad \text{or} \quad h(m_\eta) + h(m_l)\,, \tag{32}$$

will also have zero derivative at the symmetric point.

The corresponding results to Table 4 or eq. (26) are given in Tables 7, 8 and 9. We can see how well this works in practice by looking, for example at the physical masses of the decuplet baryons. If we look at the physical values of the 4 decuplet mass combinations in Table 9 and using mass values given in section 9, we get

$$\begin{array}{rcrll}
4M_\Delta + 3M_{\Sigma^*} + 2M_{\Xi^*} + M_\Omega &=& 13.82 \text{ GeV} & \text{singlet} & \propto (\delta m_l)^0 \\
-2M_\Delta \quad + M_{\Xi^*} + M_\Omega &=& 0.742 \text{ GeV} & \text{octet} & \propto \delta m_l \\
4M_\Delta - 5M_{\Sigma^*} - 2M_{\Xi^*} + 3M_\Omega &=& -0.044 \text{ GeV} & \text{27plet} & \propto \delta m_l^2 \\
-M_\Delta + 3M_{\Sigma^*} - 3M_{\Xi^*} + M_\Omega &=& -0.006 \text{ GeV} & \text{64plet} & \propto \delta m_l^3\,,
\end{array} \tag{33}$$

with a strong hierarchy in values, corresponding to the leading term in the Taylor expansion. Each additional factor of δm_l reduces the value by about an order of magnitude, the 64-plet combination is more than 2000 times smaller than the singlet combination. This suggests that the Taylor expansion converges well all the way from the symmetric point to the physical point. (Though of course it is possible that the singlet and octet curvature terms are larger than those in the 27 and 64.) Unfortunately, even with noise reduction techniques, it may be very difficult to see a signal in the 64-plet channel.

We can now 'invert' the results in Tables 8, 9 to give the expansion for each hadron mass from the symmetry point (m_0, m_0, m_0). This leads to the constrained fit formulae

$$\begin{aligned}
M_\pi^2 &= M_0^2 + 2\alpha\delta m_l + (\beta_0 + 2\beta_1)\delta m_l^2 \\
M_K^2 &= M_0^2 - \alpha\delta m_l + (\beta_0 + 5\beta_1 + 9\beta_2)\delta m_l^2 \\
M_{\eta_s}^2 &= M_0^2 - 4\alpha\delta m_l + (\beta_0 + 8\beta_1)\delta m_l^2\,,
\end{aligned} \tag{34}$$

$$\begin{aligned}
M_\rho &= M_0 + 2\alpha\delta m_l + (\beta_0 + 2\beta_1)\delta m_l^2 \\
M_{K^*} &= M_0 - \alpha\delta m_l + (\beta_0 + 5\beta_1 + 9\beta_2)\delta m_l^2 \\
M_{\phi_s} &= M_0 - 4\alpha\delta m_l + (\beta_0 + 8\beta_1)\delta m_l^2\,,
\end{aligned} \tag{35}$$

$$\begin{aligned}
M_N &= M_0 + 3A_1\delta m_l + (B_0 + 3B_1)\delta m_l^2 \\
M_\Lambda &= M_0 + 3A_2\delta m_l + (B_0 + 6B_1 - 3B_2 + 9B_4)\delta m_l^2 \\
M_\Sigma &= M_0 - 3A_2\delta m_l + (B_0 + 6B_1 + 3B_2 + 9B_3)\delta m_l^2 \\
M_\Xi &= M_0 - 3(A_1 - A_2)\delta m_l + (B_0 + 9B_1 - 3B_2 + 9B_3)\delta m_l^2\,,
\end{aligned} \tag{36}$$

$SU(3)$	Mass Combination	Expansion			
1	$3M_\pi^2 + 4M_K^2 + M_{\eta_8}^2$	1,		δm_l^2,	δm_l^3, ...
8	$-3M_\pi^2 + 2M_K^2 + M_{\eta_8}^2$		δm_l,	δm_l^2,	$\delta m l^3$, ...
27	$-M_\pi^2 + 4M_K^2 - 3M_{\eta_8}^2$			δm_l^2,	δm_l^3, ...
1	$3M_\rho + 4M_{K^*} + M_{\phi_8}$	1,		δm_l^2,	δm_l^3, ...
8	$-3M_\rho + 2M_{K^*} + M_{\phi_8}$		δm_l,	δm_l^2,	δm_l^3, ...
27	$-M_\rho + 4M_{K^*} - 3M_{\phi_8}$			δm_l^2,	δm_l^3, ...

Table 7: Meson mass combinations classified by $SU(3)$ representation, in the $2+1$ case. Octet-singlet mixing is not taken into account.

$SU(3)$	Mass Combination	Expansion			
1, 27	$2M_K^2 + M_\pi^2$	1,		δm_l^2,	δm_l^3, ...
8, 27	$M_K^2 - M_\pi^2$		δm_l,	δm_l^2,	δm_l^3, ...
1, 27	$2M_{K^*} + M_\rho$	1,		δm_l^2,	δm_l^3, ...
8, 27	$M_{K^*} - M_\rho$		δm_l,	δm_l^2,	δm_l^3, ...

Table 8: Meson mass combinations free from mixing problems, classified by $SU(3)$ representation. These combinations have been chosen to eliminate the η/η' and ω/ϕ states, so they now contain mixtures of different $SU(3)$ representations.

$SU(3)$	Mass Combination	Expansion			
1	$2M_N + 3M_\Sigma + M_\Lambda + 2M_\Xi$	1,		δm_l^2,	δm_l^3, ...
8	$M_\Xi - M_N$		δm_l,	δm_l^2,	δm_l^3, ...
8	$-M_N + 3M_\Sigma - M_\Lambda - M_\Xi$		δm_l,	δm_l^2,	δm_l^3, ...
27	$2M_N - M_\Sigma - 3M_\Lambda + 2M_\Xi$			δm_l^2,	δm_l^3, ...
1	$4M_\Delta + 3M_{\Sigma^*} + 2M_{\Xi^*} + M_\Omega$	1,		δm_l^2,	δm_l^3, ...
8	$-2M_\Delta + M_{\Xi^*} + M_\Omega$		δm_l,	δm_l^2,	δm_l^3, ...
27	$4M_\Delta - 5M_{\Sigma^*} - 2M_{\Xi^*} + 3M_\Omega$			δm_l^2,	δm_l^3, ...
64	$-M_\Delta + 3M_{\Sigma^*} - 3M_{\Xi^*} + M_\Omega$				δm_l^3, ...

Table 9: Baryon mass combinations classified by $SU(3)$ representation, in the $2+1$ case.

$$
\begin{aligned}
M_\Delta &= M_0 + 3A\delta m_l + (B_0 + 3B_1)\delta m_l^2 \\
M_{\Sigma^*} &= M_0 + 0 + (B_0 + 6B_1 + 9B_2)\delta m_l^2 \\
M_{\Xi^*} &= M_0 - 3A\delta m_l + (B_0 + 9B_1 + 9B_2)\delta m_l^2 \\
M_\Omega &= M_0 - 6A\delta m_l + (B_0 + 12B_1)\delta m_l^2 \,. \qquad (37)
\end{aligned}
$$

(The values of the constants are obviously different for each octet or decuplet.) We see that the linear terms are highly constrained. The decuplet baryons have only one slope parameter, while the octet baryons have two slope parameters. Mesons have fewer slope parameters than baryons because of constraints due to charge conjugation, again giving one slope parameter. The quadratic terms are much less constrained; indeed only for the baryon octet is there any constraint[5].

Note also that for the pseudoscalar octet, M_{η_s} is a fictitious $s\overline{s}$ particle. In the real world there is no pure $\overline{s}s$ meson (i.e. the 'strange pion') because its quarks can annihilate and mix with $\overline{u}u$ and $\overline{d}d$ to form the η, but lattice simulations can observe this η_s meson. While for the pseudoscalar octet we have non-perfect η-η' mixing, for the vector octet the situation is different. Due to near perfect mixing between the ϕ and ω the M_ϕ is (almost) a perfect $s\overline{s}$ state, so that $M_{\phi_s} \approx M_\phi$. Note also that for lattice simulations, even these fictitious particles still contain useful information, due to the constrained fit.

As eqs. (34)–(37) have been derived using only group theoretic arguments, they will be valid for results derived on any lattice volume (though the coefficients are still functions of the volume).

Finally there is the practical question of whether fits should be against the (light) quark mass or alternatively against the pseusoscalar pion mass. In Appendix C we argue that 'internally' at least the fits should be made against the quark mass. Of course this is only a useful observation when quadratic or higher terms are involved. To leading order eqs. (35)–(37) can be written as

$$
\delta M \equiv M - M_0 = c_M \delta m_l \,, \qquad (38)
$$

(together with $\delta M^2 \equiv M^2 - M_0^2 = c_M \delta m_l$ in the case of pseudoscalar mesons, eq. (34)). The coefficients c_M can be found from these equations. Thus an expansion in δm_l is equivalent to an expansion in δM or δM^2.

4 Applications to chiral perturbation theory

Almost all leading order χPT results follow simply from flavour blindness, without any input from chiral symmetry. The linear terms in m_q, which are usually called

[5]The coefficients of the δm_l^2 terms appear complicated; indeed there seem to be too many for the baryon octet, eq. (36). In section 5 we generalise these formulae to the case of different valence quark masses to sea quark masses or 'partially quenching' when this choice of coefficients becomes relevant.

LO χPT results, were originally discovered by Gell-Mann and Okubo [10, 11], using the (non-chiral) $SU(3)$ argument we are using in this article.

The only case where we need to invoke chiral symmetry is for the pseudoscalar meson mass formula, where it is chiral symmetry which tells us that we have massless Goldstone bosons if 2 or more quark masses vanish.

Beyond leading order we cannot derive the χPT result in full solely from flavour blindness, but we can still make useful statements about the form that higher order contributions must take.

4.1 Decuplet baryon masses at $\mathbf{O(M^{3/2})}$

$O(M^{3/2})$ χPT is based on one-loop graphs, all with a pseudo-Goldstone boson. So we should expect that the individual terms in the χPT answer will be functions of M_π or of M_K or of M_η, with no mixed terms (such as $M_\pi^2 M_K^2$), which can only arise at the two-loop level.

As an example, let us examine the NLO results for the decuplet baryon masses, [15]. Taking the formulae for individual masses, and grouping them into the multiplets of Table 9, we know that in each case we are only allowed chiral perturbation theory expressions in the corresponding multiplet:

$$\begin{aligned} 4M_\Delta + 3M_{\Sigma^*} + 2M_{\Xi^*} + M_\Omega &= 10M_0 + 20(\gamma_M - 3\overline{\sigma}_M)\overline{m} \\ &\quad -\frac{5\mathcal{H}^2}{72\pi f^2}\,\frac{5}{3}\left[3M_\pi^3 + 4M_K^3 + M_\eta^3\right] \\ &\quad -\frac{\mathcal{C}^2}{(4\pi f)^2}\,\frac{5}{3}\left[3\mathcal{F}_-(M_\pi) + 4\mathcal{F}_-(M_K) + \mathcal{F}_-(M_\eta)\right] \end{aligned} \tag{39}$$

$$\begin{aligned} -2M_\Delta + M_{\Xi^*} + M_\Omega &= -10\gamma_M \delta m_l \\ &\quad -\frac{5\mathcal{H}^2}{72\pi f^2}\,\frac{1}{2}\left[-3M_\pi^3 + 2M_K^3 + M_\eta^3\right] \\ &\quad -\frac{\mathcal{C}^2}{(4\pi f)^2}\,\frac{1}{3}\left[-3\mathcal{F}_-(M_\pi) + 2\mathcal{F}_-(M_K) + \mathcal{F}_-(M_\eta)\right] \end{aligned} \tag{40}$$

$$\begin{aligned} 4M_\Delta - 5M_{\Sigma^*} - 2M_{\Xi^*} + 3M_\Omega &= \frac{5\mathcal{H}^2}{72\pi f^2}\,\frac{7}{9}\left[-M_\pi^3 + 4M_K^3 - 3M_\eta^3\right] \\ &\quad -\frac{\mathcal{C}^2}{(4\pi f)^2}\,\frac{7}{9}\left[-\mathcal{F}_-(M_\pi) + 4\mathcal{F}_-(M_K) - 3\mathcal{F}_-(M_\eta)\right] \end{aligned} \tag{41}$$

$$-M_\Delta + 3M_{\Sigma^*} - 3M_{\Xi^*} + M_\Omega = 0\,, \tag{42}$$

where $\mathcal{F}_-(M_i)$ is short-hand for the function $\mathcal{F}(M_i, -\Delta, \mu)$ defined in [15]. We see that on the right-hand side we only get meson combinations of the same symmetry as we have on the left-hand side, for example in the 27-plet case, eq. (41), all the terms on the right-hand side have the structure of the mesonic 27-plet of Table 7.

We proved a weaker version of this result in [1], using the permutation group instead of full $SU(3)$.

The meson mass matrix, $8 \otimes 8$, contains no 64, there are no possible 1-loop terms to place on the right-hand side of eq. (42), so this mass combination must be zero in NLO χPT. We have already noted in Table 9 that this combination has a Taylor expansion beginning at $O(\delta m_l^3)$ and is very small experimentally, eq. (33).

4.2 Relationships between expansion coefficients

Finally we show that there is a relation between the parameters of χPT and the Taylor coefficients in our approach, eqs. (34) – (37).

For example for the pseudoscalar octet, using the results in [18] and assuming their validity up to the point on the flavour symmetric line, we find

$$\begin{aligned}
M_0^2 &= \overline{\chi}\left[1 - \frac{16\overline{\chi}}{f_0^2}\left(3L_4 + L_5 - 6L_6 - 2L_8\right) + \frac{\overline{\chi}}{24\pi^2 f_0^2}\ln\frac{\overline{\chi}}{\Lambda_\chi^2}\right] \\
\alpha &= Q_0\left[1 - \frac{16\overline{\chi}}{f_0^2}\left(3L_4 + 2L_5 - 6L_6 - 4L_8\right) + \frac{\overline{\chi}}{8\pi^2 f_0^2}\ln\frac{\overline{\chi}}{\Lambda_\chi^2}\right] \\
\beta_0 &= -\frac{Q_0^2}{6\pi^2 f_0^2} \\
\beta_1 &= \frac{Q_0^2}{f_0^2}\left[-32\left(L_5 - 2L_8\right) + \frac{1}{24\pi^2}\left(7 + 4\ln\frac{\overline{\chi}}{\Lambda_\chi^2}\right)\right] \\
\beta_2 &= \frac{Q_0^2}{f_0^2}\left[16\left(L_5 - 2L_8\right) - \frac{1}{24\pi^2}\left(3 + 2\ln\frac{\overline{\chi}}{\Lambda_\chi^2}\right)\right], \qquad (43)
\end{aligned}$$

with $Q_0 = B_0^R Z_m^{NS}$, $\overline{\chi} = 2Q_0(1+\alpha_z)\overline{m}$, where the L_is are appropriate Low Energy Constants or LECs.

We first note that when expanding the χPT about a point on the $SU(3)$ flavour symmetry line gives, as expected, to leading order only one parameter, α. (This means, in particular, that flavour singlet combinations, X_S, vanish to leading order, as discussed previously.) Secondly, while we can fit to α and β_0, β_1 and β_2, it will be difficult to determine the individual LECs. The best we can probably hope for are these combinations.

5 Partial quenching

In Partial Quenching (PQ) measurements are made with the mass of the valence quarks different from the sea quarks. In this case the sea quark masses m_l, m_s remain constrained by $\overline{m} = \text{const.}$, but the valence quark masses μ_l, μ_s are unconstrained. We define

$$\delta\mu_q = \mu_q - m_0\,, \quad q = l, s\,. \qquad (44)$$

When $\mu \to m$ (i.e. return to the 'unitary line') then the following results collapse to the previous results of eqs. (34) – (37). In the following we sketch some results, see [17] for more details.

5.1 PQ decuplet baryons

In the partially quenched case we know that the hadron mass formulae should have an $SU(3)$ symmetry for interchanging the sea quarks, and another $SU(3)$ symmetry for operations on the valence quarks. The sea quark symmetry will always be singlet, the valence quark terms for a hadron in the irreducible representation N can be in any representation which occurs in $\overline{N} \otimes N$.

Let us see what sort of mass relations symmetry allows us, taking the decuplet baryons as our example. Starting with linear terms in the quark masses, we can form two polynomials of the valence masses, a singlet combination $(2\delta\mu_l + \delta\mu_s)$ and an octet combination with E^+ symmetry, $(\delta\mu_s - \delta\mu_l)$. (A first-order term in the sea quark masses is ruled out because we are keeping $2m_l + m_s$ constant.) We can read off the coefficients each polynomial must have from Fig. 8. So, at first sight we would expect

$$\begin{aligned} M_\Delta &= M_0 + \alpha_1(2\delta\mu_l + \delta\mu_s) - \alpha_2(\delta\mu_s - \delta\mu_l) \\ M_{\Sigma^*} &= M_0 + \alpha_1(2\delta\mu_l + \delta\mu_s) \\ M_{\Xi^*} &= M_0 + \alpha_1(2\delta\mu_l + \delta\mu_s) + \alpha_2(\delta\mu_s - \delta\mu_l) \\ M_\Omega &= M_0 + \alpha_1(2\delta\mu_l + \delta\mu_s) + 2\alpha_2(\delta\mu_s - \delta\mu_l)\,, \end{aligned} \tag{45}$$

with no connection between α_1 and α_2. However, it is clear that the Δ mass can not know anything about the strange valence mass, and the Ω mass must similarly be independent of $\delta\mu_l$. These constraints are both satisfied if

$$\alpha_1 = \alpha_2 \equiv A\,, \tag{46}$$

giving us a leading-order formula

$$\begin{aligned} M_\Delta &= M_0 + 3A\delta\mu_l \\ M_{\Sigma^*} &= M_0 + A(2\delta\mu_l + \delta\mu_s) \\ M_{\Xi^*} &= M_0 + A(\delta\mu_l + 2\delta\mu_s) \\ M_\Omega &= M_0 + 3A\delta\mu_s\,. \end{aligned} \tag{47}$$

We can continue this procedure to the quadratic level. Again, the number of terms is reduced by keeping the sum of the sea quark masses fixed; and we again find the number of coefficients reduced by the constraint that the Δ mass is independent of $\delta\mu_s$, and the Ω mass independent of $\delta\mu_l$. We obtain the quadratic results

$$M_\Delta = M_0 + 3A\delta\mu_l + B_0\delta m_l^2 + 3B_1\delta\mu_l^2$$

$$
\begin{aligned}
M_{\Sigma^*} &= M_0 + A(2\delta\mu_l + \delta\mu_s) + B_0\delta m_l^2 + B_1(2\delta\mu_l^2 + \delta\mu_s^2) + B_2(\delta\mu_s - \delta\mu_l)^2 \\
M_{\Xi^*} &= M_0 + A(\delta\mu_l + 2\delta\mu_s) + B_0\delta m_l^2 + B_1(\delta\mu_l^2 + 2\delta\mu_s^2) + B_2(\delta\mu_s - \delta\mu_l)^2 \\
M_{\Omega} &= M_0 + 3A\delta\mu_s + B_0\delta m_l^2 + 3B_1\delta\mu_s^2 \,. \qquad (48)
\end{aligned}
$$

These formulae apply when the sum of the sea quark masses are held constant, $\frac{1}{3}(2m_l + m_s) = m_0$, but the valence quark masses are completely free, because at this level (terms up to second order) a restriction on valence masses would not lead to any reduction in the number of free parameters.

Let us use these formulae to illustrate how partially quenched measurements might help us fit masses on the constant sea-quark line. In these equations, M_Δ and M_Ω are fully unquenched baryon masses along the constant sea-quark line $\frac{1}{3}(2m_l + m_s) = m_0$, and M_Δ^{PQ} is a partially quenched Δ, measured on the symmetric configuration $m_l = m_s = m_0$. From eq. (48) we can read off the relevant mass relations

$$
\begin{aligned}
M_\Delta &= M_0 + 3A\delta m_l + (B_0 + 3B_1)\delta m_l^2 \qquad && -m_0^R < \delta m_l^R < \tfrac{1}{2}m_0^R \\
M_\Omega &= M_0 + 3A\delta m_s + (\tfrac{1}{4}B_0 + 3B_1)\delta m_s^2 \qquad && -m_0^R < \delta m_s^R < 2m_0^R \\
M_\Delta^{PQ} &= M_0 + 3A\delta\mu_l + 3B_1\delta\mu_l^2 && -m_0^R < \delta\mu_l^R \,. \qquad (49)
\end{aligned}
$$

The unquenched quark masses can only be varied through a rather small range, but the partially quenched quark mass can be varied much further, giving us a better lever-arm to measure curvatures. Data on the partially quenched Δ could give the parameters A and B_1, which would predict the Ω-Δ splitting and the Ξ-Σ splitting in the fan plot. We could also find the parameter B_2 by looking at mixed-mass partially quenched decuplet baryons.

There are some combinations of the partially quenched masses, eqs. (48) which have simpler dependences on the valence quark masses. Examples include

$$
\begin{aligned}
-M_\Delta + M_{\Sigma^*} + M_{\Xi^*} - M_\Omega &= 2B_2(\delta\mu_s - \delta\mu_l)^2 \\
M_{\Xi^*} - M_{\Sigma^*} &= A(\delta\mu_s - \delta\mu_l) + B_1(\delta\mu_s^2 - \delta\mu_l^2) \\
M_\Omega - M_\Delta &= 3A(\delta\mu_s - \delta\mu_l) + 3B_1(\delta\mu_s^2 - \delta\mu_l^2) \,. \qquad (50)
\end{aligned}
$$

5.2 PQ octet mesons

The mass formulae for mesons takes the form:

$$
\begin{aligned}
M_\pi^2 &= M_0^2 + 2\alpha\delta\mu_l + \beta_0\delta m_l^2 + 2\beta_1\delta\mu_l^2 \\
M_K^2 &= M_0^2 + \alpha(\delta\mu_l + \delta\mu_s) + \beta_0\delta m_l^2 + \beta_1(\delta\mu_l^2 + \delta\mu_s^2) + \beta_2(\delta\mu_s - \delta\mu_l)^2 \\
M_{\eta_s}^2 &= M_0^2 + 2\alpha\delta\mu_s + \beta_0\delta m_l^2 + 2\beta_1\delta\mu_s^2 \,. \qquad (51)
\end{aligned}
$$

Again the η_s is the meson made of a partially quenched $\overline{s}_{val}s_{val}$ quarks, (i.e. the 'strange pion') which in the partially quenched framework can be observed

and can yield useful information about the extrapolation constants. Some useful combinations, which avoid the delicate η sector, are

$$\begin{aligned} M_K^2 - M_\pi^2 &= \alpha(\delta\mu_s - \delta\mu_l) + \beta_1(\delta\mu_s^2 - \delta\mu_l^2) + \beta_2(\delta\mu_s - \delta\mu_l)^2 \\ 2M_K^2 + M_\pi^2 &= 3M_0^2 + \alpha(4\delta\mu_l + 2\delta\mu_s) + 3\beta_0\delta m_l^2 \\ &\quad +\beta_1(4\delta\mu_l^2 + 2\delta\mu_s^2) + 2\beta_2(\delta\mu_s - \delta\mu_l)^2 \,. \end{aligned} \tag{52}$$

$M_K^2 - M_\pi^2$ is useful as a measure of the quark mass splitting, $2M_K^2 + M_\pi^2$ as a quantity which is nearly constant along our trajectory.

The same form, mutatis mutandis, applies to the other meson octets, e.g. the ρ, K^*, ϕ system. We thus have

$$\begin{aligned} M_\rho &= M_0 + 2\alpha\delta\mu_l + \beta_0\delta m_l^2 + 2\beta_1\delta\mu_l^2 \\ M_{K^*} &= M_0 + \alpha(\delta\mu_l + \delta\mu_s) + \beta_0\delta m_l^2 + \beta_1(\delta\mu_l^2 + \delta\mu_s^2) + \beta_2(\delta\mu_s - \delta\mu_l)^2 \\ M_\phi &= M_0 + 2\alpha\delta\mu_s + \beta_0\delta m_l^2 + 2\beta_1\delta\mu_s^2 \,, \end{aligned} \tag{53}$$

following the pattern of eq. (51).

5.3 PQ octet baryons

The number of free coefficients in the meson case was reduced by the requirement that K and $\overline{K}$ have the same masses, there is no similar constraint linking N and Ξ, so more coefficients are allowed, both at the linear and quadratic levels. We find

$$\begin{aligned} M_N &= M_0 + 3A_1\delta\mu_l + B_0\delta m_l^2 + 3B_1\delta\mu_l^2 \\ M_\Lambda &= M_0 + A_1(2\delta\mu_l + \delta\mu_s) - A_2(\delta\mu_s - \delta\mu_l) + B_0\delta m_l^2 \\ &\quad +B_1(2\delta\mu_l^2 + \delta\mu_s^2) - B_2(\delta\mu_s^2 - \delta\mu_l^2) + B_4(\delta\mu_s - \delta\mu_l)^2 \\ M_\Sigma &= M_0 + A_1(2\delta\mu_l + \delta\mu_s) + A_2(\delta\mu_s - \delta\mu_l) + B_0\delta m_l^2 \\ &\quad +B_1(2\delta\mu_l^2 + \delta\mu_s^2) + B_2(\delta\mu_s^2 - \delta\mu_l^2) + B_3(\delta\mu_s - \delta\mu_l)^2 \\ M_\Xi &= M_0 + A_1(2\delta\mu_l + \delta\mu_s) - A_2(\delta\mu_s - \delta\mu_l) + B_0\delta m_l^2 \\ &\quad +B_1(\delta\mu_l^2 + 2\delta\mu_s^2) - B_2(\delta\mu_s^2 - \delta\mu_l^2) + B_3(\delta\mu_s - \delta\mu_l)^2 \,. \end{aligned} \tag{54}$$

As usual, the nucleon mass has been made independent of $\delta\mu_s$. Some useful combinations, which only depend on a few parameters, are

$$\begin{aligned} 2M_N - M_\Sigma - 3M_\Lambda + 2M_\Xi &= (B_3 - 3B_4)(\delta\mu_s - \delta\mu_l)^2 \qquad (55) \\ M_\Xi - M_\Sigma &= (A_1 - 2A_2)(\delta\mu_s - \delta\mu_l) + (B_1 - 2B_2)(\delta\mu_s^2 - \delta\mu_l^2) \,. \end{aligned}$$

As mentioned previously, we can check that when $\mu \to m$ (i.e. return to the 'unitary line') then these results return to the previous results of eqs. (34) – (37).

5.4 The potential usefullness of PQ

There are several possible advantages to considering PQ results.

1. The coefficients that appear in the expansions about the flavour symmetric line in the PQ case are the same as those that appear on the 'unitary' case. Hence this may be a computationally cheaper way of obtaining them.

2. PQ results can be helpful in choosing the next point to simulate, because the meson masses measured in the partially quenched approximation are very close to those found in a full calculation, giving us a preview of results on the next simulation point. We understand theoretically why this works well on our trajectory, with $\overline{m}$ held fixed. The reason is that the effect on the sea of making the u and d quarks lighter is largely cancelled by the effect of making the s quark heavier (the cancellation is perfect at the flavour symmetric point). Therefore partially quenching works best when only the non-singlet part of the quark mass matrix is varied (as is the case here). If the singlet part (the average sea-quark mass) is changed, there is no compensation, and the partial quenched results are less reliable.

3. We can use partial quenching to get a good estimate of results at the physical point, by taking configurations generated with quark masses some distance short of the physical point, and then at the measurement stage using valence quarks chosen to give the physical π and K masses. Important physical effects, such as the light pion cloud, would be incorporated in the results. The effects of partially quenching can be further reduced by repeating the calculation with several choices of sea-quark masses, and making an extrapolation towards the physical sea-quark mass values.

We can also show that on this trajectory the errors of the partially quenched approximation are much smaller than on other trajectories. In leading order χPT (terms linear in the quark mass), the suggested procedure (valence quarks at the physical value, sea quarks anywhere on the physical constant $\overline{m}_{sea}$) is exact. See Table VIII of [16] for the leading order formulae for both octet and decuplet baryon masses. At this order partial quenching moves all the octet baryons by the same amount, and all decuplets also move together. The leading order partial quenching errors are

$$\begin{aligned} M_{oct}^{PQ} - M_{oct}^{phys} &= 6\sigma_M(\overline{m}_{sea}^{lat} - \overline{m}_{sea}^{phys}) \\ M_{dec}^{PQ} - M_{dec}^{phys} &= -6\overline{\sigma}_M(\overline{m}_{sea}^{lat} - \overline{m}_{sea}^{phys})\,, \end{aligned} \tag{56}$$

(using [16] notation for quark masses and the σ coefficients). Since we have tuned $\overline{m}_{sea}^{lat}$ to be equal to the physical value, the partial quenching error vanishes on our trajectory, but not on other trajectories, which vary $\overline{m}_{sea}^{lat}$.

We can give a partial derivative argument, like that of section 1 or [1], which explains why this is so. Take the proton mass as an example, but any quantity will work the same way. The proton mass will depend on the valence quark masses and the sea quark masses, so we can write

$$M_p^{PQ}(m_u^{val}, m_d^{val}; m_u^{sea}, m_d^{sea}, m_s^{sea})\,. \tag{57}$$

The dependence on the three sea masses must be completely symmetrical, unlike the dependence on valence masses. At the symmetric point

$$\frac{\partial M_p^{PQ}}{\partial m_u^{sea}} = \frac{\partial M_p^{PQ}}{\partial m_d^{sea}} = \frac{\partial M_p^{PQ}}{\partial m_s^{sea}}\,, \tag{58}$$

so if the sea quark masses are changed in a way which preserves $\overline{m}^{sea}$, while the valence masses are held constant, M_p^{PQ} will not change (to leading order).

6 The path to the physical point

In section 1 the proposed path to the physical point was introduced. We shall now discuss this a little further.

For the simulation it is easiest to keep the (bare) singlet quark mass fixed,

$$\overline{m} = \tfrac{1}{3}(2m_l + m_s) = m_0 = \text{const.}\,, \tag{59}$$

starting from some reference point (m_0, m_0) on the flavour symmetric line. We can use the singlet combinations from Table 6 to locate the starting point of our path to the physical point by fixing a dimensionless ratio such as

$$\frac{X_\pi^2}{X_N^2} = \text{physical value}\,. \tag{60}$$

Note also that $X_\pi = m_\pi|_0$ at the flavour symmetric point so this determines our starting pion mass from Table 11 to be $\sim 410\,\text{MeV}$.

However this is only strictly true at lowest order. While at this order it does not matter whether we kept the quark mass singlet constant, eq. (59), or a particle mass singlet constant, eq. (60), higher order terms mean that it now does. If we make different choices of the quantity we keep constant at the experimentally measured physical value, for example

$$\frac{X_\pi^2}{X_N^2}\,, \quad \frac{X_\pi^2}{X_\Delta^2}\,, \quad \frac{X_\pi^2}{X_\rho^2}\,, \quad \ldots\,, \tag{61}$$

we get slightly different trajectories. The different trajectories begin at slightly different points along the flavour $SU(3)$ symmetric line. Initially they are all parallel with slope -2, but away from the symmetry line they can curve, and will

all meet at the physical point. (Numerically we shall later see that this seems to be a small effect.)

An additional effect comes from the choice of Wilson lattice fermions (for chiral fermions there is no effect). The physical domain is defined by

$$\begin{aligned} m_l^R &\geq 0 \\ m_s^R &\geq 0\,, \end{aligned} \tag{62}$$

which using eq. (5) translates to

$$m_l \geq -\frac{\frac{1}{3}\alpha_Z}{(1+\frac{2}{3}\alpha_Z)} m_s\,, \qquad m_s \geq -\frac{\frac{2}{3}\alpha_Z}{(1+\frac{1}{3}\alpha_Z)} m_l\,, \tag{63}$$

leading to non-orthogonal axes and possibly negative bare quark mass. (These features disappear of course for chiral fermions when $\alpha_Z = 0$.)

These two features are sketched in Fig. 9, which shows possible paths in the

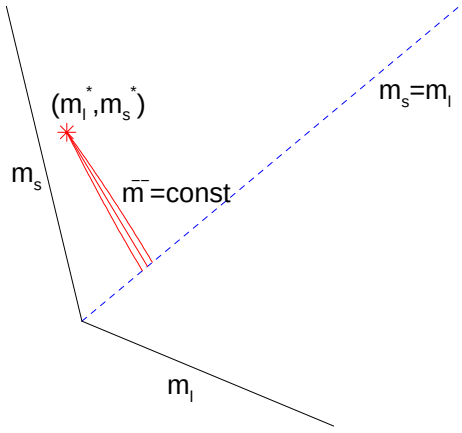

Figure 9: Sketch of some possible paths (red lines) in the (m_l, m_s) plane to the physical point (m_l^*, m_s^*).

(m_l, m_s) plane starting from the flavour symmetric line.

7 The lattice – generalities

After the general discussion of $SU(3)$ flavour expansions described in sections 2–5 (which are lattice independent) we now turn to more specific lattice considerations.

7.1 Lattice simulations

We use a clover action for $2+1$ flavours with a single iterated mild stout smearing as described in Appendix D. Further details are given in [19] together with a non-perturbative determination of the improvement coefficient for the clover term, using the Schrödinger functional method.

The bare quark masses are defined as

$$am_q = \frac{1}{2}\left(\frac{1}{\kappa_q} - \frac{1}{\kappa_{0;c}}\right) , \tag{64}$$

where vanishing of the quark mass along the $SU(3)$ flavour symmetric line determines $\kappa_{0;c}$. We then keep $\overline{m} = \text{const.} \equiv m_0$ which gives

$$\kappa_s = \frac{1}{\frac{3}{\kappa_0} - \frac{2}{\kappa_l}} . \tag{65}$$

So once we decide on a κ_l this then determines κ_s.

Furthermore note that we are not expanding about the chiral limit, but have expansions around a flavour symmetric point which does not require a knowledge of $\kappa_{0;c}$. This follows as

$$\begin{aligned} \delta m_q &= m_q - m_0 \\ &= \frac{1}{2a}\left(\frac{1}{\kappa_q} - \frac{1}{\kappa_0}\right) . \end{aligned} \tag{66}$$

HMC and RHMC were used for the 2 and 1 fermion flavours respectively, [20], to generate the gauge configurations. We note the following in connection with the simulations and our path choice:

- HMC simulations should equilibriate quickly from one point to another along this path.
- The HMC cost change should be moderate for this path. This may be motivated by the following crude cost argument. Modelling the HMC cost, C, as

  $$C \propto \frac{1}{am_l^R} + \frac{k}{am_s^R} , \tag{67}$$

  gives on the line $a\overline{m} = \text{const} = am_0$

  $$C \propto \frac{1}{\alpha_Z + \xi} + \frac{k}{(3+\alpha_Z) - 2\xi} , \tag{68}$$

  with

  $$\xi = \frac{m_l}{m_0} . \tag{69}$$

  This is plotted in Fig. 10. There is little change in a reasonably large range of ξ starting from $\xi = 1$.

Both these points are indeed found in practice (at least approximately).

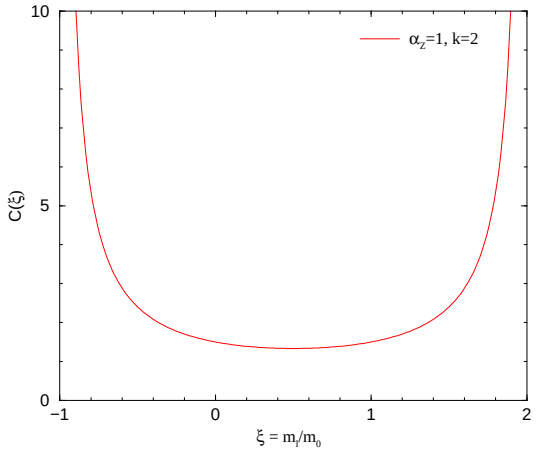

Figure 10: Simulation cost $C(\xi)$ against ξ where $\xi = m_l/m_0$ (with, for example, $\alpha_Z = 1$ and $k = 2$).

7.2 O(a)-improvement of the coupling constant

$O(a)$-improvement leads to a change in the coupling constant (or β) via

$$g_0^2 \to \tilde{g}_0^2 = g_0^2 \left(1 + b_g a\overline{m}\right), \tag{70}$$

where b_g is some function of g_0^2. In general when we vary a quark mass then g_0 must be changed to keep $\tilde{g}_0$ constant. However for our choice of path ($\overline{m} = \text{const.}$) the relation between g_0 and $\tilde{g}_0$ is *fixed*, so only a small overall shift of results might be necessary – nothing else changes as we traverse our path.

Not much is known about the value of b_g. For Wilson glue and $\alpha = 0$ (i.e. no-stout smeared links) Wilson-Dirac fermions the lowest order perturbative result is $b_g = 0.01200 n_f g_0^2 + O(g_0^4)$, [21], which is small but increasing with n_f (here $n_f = 3$). A crude estimate was made in [22] and indicated a possible 1–2% effect (but with considerable uncertainty). In the following we shall not consider the effect of b_g any further.

7.3 Hadron 'wavefunctions'

The operators (wave functions) used to determine the hadron masses are uniformly taken to be Jacobi smeared ([23] and [24] (Appendix C)) and to be non-relativistic, NR, ([25], [26] and [27] (Appendix C)). Specifically, we consider the following hadron wave functions:

- Pseudoscalar meson octet

$$\begin{aligned} M_\pi(x) &= \overline{d}(x)\gamma_5 u(x) \\ M_K(x) &= \overline{s}(x)\gamma_5 u(x) \\ M_{\eta_s}(x) &= \overline{s}(x)\gamma_5 s(x) \end{aligned} \tag{71}$$

- Vector meson octet

$$\begin{aligned} M_{\rho\,i}(x) &= \overline{d}(x)\gamma_i u(x) \\ M_{K^*\,i}(x) &= \overline{s}(x)\gamma_i u(x) \\ M_{\phi_s\,i}(x) &= \overline{s}(x)\gamma_i s(x) \end{aligned} \tag{72}$$

- Baryon octet

$$\begin{aligned} B_{N\,\alpha}(x) &= \epsilon_{abc} u^a_\alpha(x) \left[u^b(x)^{T_D} C\gamma_5 d^c(x)\right] \\ B_{\Lambda\,\alpha}(x) &= \epsilon_{abc} \left(2s^a_\alpha(x) \left[u^b(x)^{T_D} C\gamma_5 d^c(x)\right]\right. \\ &\quad \left. + d^a_\alpha(x) \left[u^b(x)^{T_D} C\gamma_5 s^c(x)\right] - u^a_\alpha(x) \left[d^b(x)^{T_D} C\gamma_5 s^c(x)\right]\right) \\ B_{\Sigma\,\alpha}(x) &= \epsilon_{abc} u^a_\alpha(x) \left[u^b(x)^{T_D} C\gamma_5 s^c(x)\right] \\ B_{\Xi\,\alpha}(x) &= \epsilon_{abc} s^a_\alpha(x) \left[s^b(x)^{T_D} C\gamma_5 u^c(x)\right] \end{aligned} \tag{73}$$

- Baryon decuplet

$$\begin{aligned} B_{\Delta\,i\alpha}(x) &= \epsilon_{abc} \left(2u^a_\alpha(x) \left[u^b(x)^{T_D} C\gamma_- d^c(x)\right] + d^a_\alpha(x) \left[u^b(x)^{T_D} C\gamma_- u^c(x)\right]\right) \\ B_{\Sigma^*\,\alpha}(x) &= \epsilon_{abc} \left(2u^a_\alpha(x) \left[u^b(x)^{T_D} C\gamma_- s^c(x)\right] + s^a_\alpha(x) \left[u^b(x)^{T_D} C\gamma_- u^c(x)\right]\right) \\ B_{\Xi^*\,\alpha}(x) &= \epsilon_{abc} \left(2s^a_\alpha(x) \left[s^b(x)^{T_D} C\gamma_- u^c(x)\right] + u^a_\alpha(x) \left[s^b(x)^{T_D} C\gamma_- s^c(x)\right]\right) \\ B_{\Omega\,\alpha}(x) &= \epsilon_{abc} s^a_\alpha(x) \left[s^b(x)^{T_D} C\gamma_- s^c(x)\right] \end{aligned} \tag{74}$$

where $C = \gamma_2\gamma_4$ and $\gamma_- = \frac{1}{2}(\gamma_2 + i\gamma_1)$ and ^{T_D} is a transpose in Dirac space. The u and d quarks are considered as distinct, but of degenerate mass.

The correlation functions (on a lattice of temporal extension T) we use are given by

$$\begin{aligned} C_{\pi_O}(t) &= \frac{1}{V_s} \left\langle \sum_{\vec{y}} M_{\pi_O}(\vec{y},t) \sum_{\vec{x}} M_{\pi_O}(\vec{x},0) \right\rangle \\ &\propto A\left(e^{-M_{\pi_O} t} + e^{-M_{\pi_O}(T-t)}\right), \qquad \pi_O = \pi, K, \eta_s \\ C_{\rho_O}(t) &= \frac{1}{3V_s} \sum_i \left\langle \sum_{\vec{y}} M_{\rho_O\,i}(\vec{y},t) \sum_{\vec{x}} M_{\rho_O\,i}(\vec{x},0) \right\rangle \\ &\propto A\left(e^{-M_{\rho_O} t} + e^{-M_{\rho_O}(T-t)}\right), \qquad \rho_O = \rho, K^*, \phi_s \\ C_{N_O}(t) &= \frac{1}{V_s} \mathrm{Tr}_D \Gamma_{unpol} \left\langle \sum_{\vec{y}} B_{N_O}(\vec{y},t) \sum_{\vec{x}} B_{N_O}(\vec{x},0) \right\rangle \\ &\propto A e^{-M_{N_O} t} + B e^{-M'_{N_O}(T-t)}, \qquad N_O = N, \Sigma, \Xi \\ C_{N_\Lambda}(t) &= \frac{1}{V_s} \mathrm{Tr}_D \Gamma_{pol} \left\langle \sum_{\vec{y}} B_{N_\Lambda}(\vec{y},t) \sum_{\vec{x}} B_{N_\Lambda}(\vec{x},0) \right\rangle \end{aligned}$$

$$
\begin{aligned}
&\propto \quad Ae^{-M_{N_\Lambda} t} + Be^{-M'_{N_\Lambda}(T-t)}\,, \\
C_{\Delta_O}(t) &= \frac{1}{V_s}\,\mathrm{Tr}_D\Gamma_{pol}\left\langle \sum_{\vec{y}} B_{\Delta_O}(\vec{y},t)\sum_{\vec{x}} B_{\Delta_O}(\vec{x},0)\right\rangle \\
&\propto \quad Ae^{-M_{\Delta_O} t} + Be^{-M'_{\Delta_O}(T-t)}\,, \qquad \Delta_O = \Delta,\Sigma^*,\Xi^*,\Omega
\end{aligned}
\tag{75}
$$

with $\Gamma_{unpol} = \frac{1}{2}(1+\gamma_4)$ and $\Gamma_{pol} = \Gamma_{unpol}(1+i\gamma_3\gamma_5)$. M' is the lowest excited state with opposite parity to M.

8 The lattice – results

All the results given in this article will be at $\beta \equiv 10/g_0^2 = 5.50$, $\alpha = 0.1$, together with $c_{sw} = 2.65$, see Appendix D. (This β value was located by an initial series of short degenerate quark mass runs, to give a rough idea of the associated scale.)

8.1 Locating κ_0 and the $\mathbf{m_s^R}$–$\mathbf{m_l^R}$ plane

From the discussion in section 6 for our path choice, we must first determine the starting value on the flavour symmetric line. A series of runs along the $SU(3)$ flavour line determines this point, κ_0, by looking when X_π^2/X_S^2, $S = N$, Δ, ρ are equal to their physical values, see eqs. (60), (61). (This would also include $S = r$ if we have previously determined the physical value of r_0.) On the flavour symmetric line obviously all the particles in the multiplet are mass degenerate, so for example taking $S = N$ means that

$$
\frac{(am_\pi)^2}{(am_N)^2} = \left.\frac{X_\pi^2}{X_N^2}\right|^*\,, \tag{76}
$$

where, to emphasise that the left-hand side are the lattice measurements, we temporarily include the lattice spacing.

Once we have located a promising κ_0 (or better a small range of κ_0s) then we keep $\overline{m}$ = const. and pick appropriate (κ_l, κ_s) values, using eq. (65). Again setting X_π^2/X_N^2 = physical value eq. (60) can be re-written as

$$
\frac{2M_K^2 - M_\pi^2}{X_N^2} = c_N + 2\frac{M_\pi^2}{X_N^2}\,, \qquad c_N = 3\left.\frac{X_\pi^2}{X_N^2}\right|^*\,, \tag{77}
$$

considering for the present only lowest order in the flavour expansion. In Fig. 11 we plot $(2m_K^2 - m_\pi^2)/X_N^2$ versus M_π^2/X_N^2. This is equivalent to a plot of the m_l^R-m_s^R plane. (The runs on $24^3\times 48$ lattices have $O(2000)$ trajectories, while the runs on $32^3\times 64$ lattices have $O(1500)$ trajectories.) Note that simulations with a 'light' strange quark mass and heavy 'light' quark mass are possible – here the right most points. In this inverted strange world we would expect $p \to \Sigma$ or Λ decays.

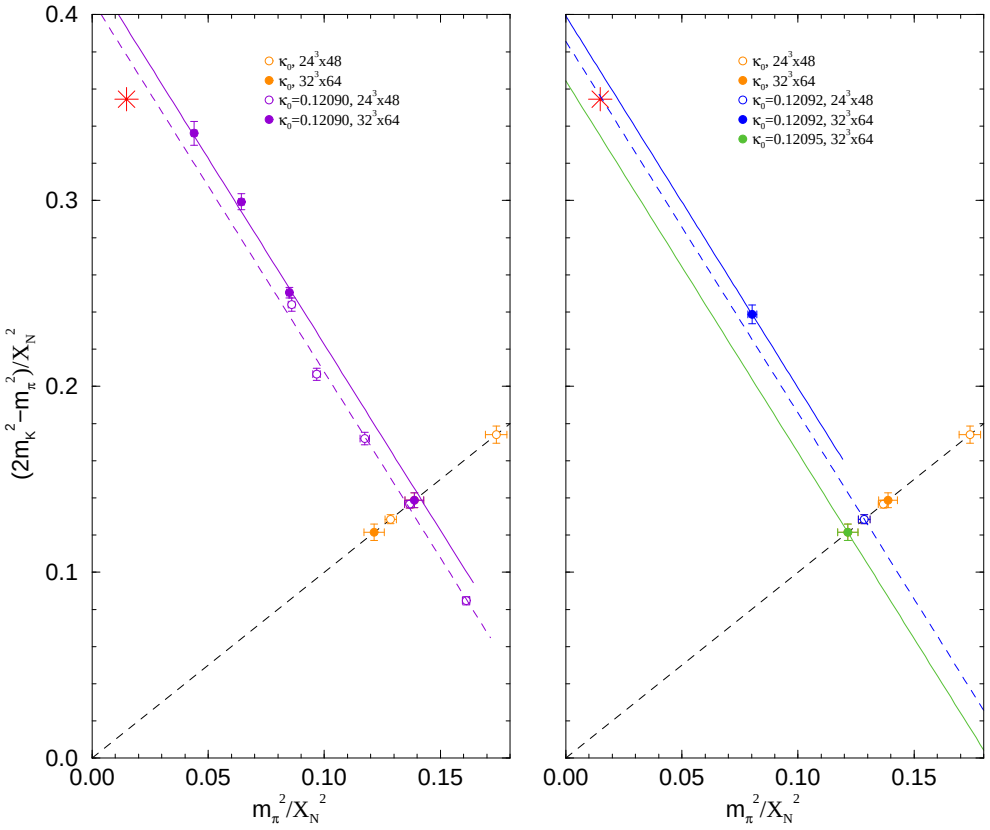

Figure 11: $(2m_K^2 - m_\pi^2)/X_N^2$ versus M_π^2/X_π^2 for $\kappa_0 = 0.12090$ (left panel) and 0.12092, 0.12095 (right panel). The dashed black line, $y = x$ represents the $SU(3)$ flavour symmetric line. Filled points are on $32^3 \times 64$ lattices while open points are on a $24^3 \times 48$ sized lattice. Shown are points on the flavour symmetric line (orange) followed by results with $\overline{m} = \text{const}$. The fits are from eq. (77) with c_N a free parameter. Physical values are denoted by stars.

Also shown in Fig. 11 are fits using eq. (77) leaving c_N as a free parameter starting from the flavour symmetric points

$$\kappa_0 = 0.12090\,, \quad \kappa_0 = 0.12092\,, \quad \kappa_0 = 0.12095\,, \tag{78}$$

(the latter two points are reference points.) It is seen from the figure that this range covers the possible paths to the physical point. There are two observations to be made. Firstly we note that there does not seem to be much non-linearity in the data, i.e. the leading order in the expansion about the flavour symmetric line already seems sufficient. So if $c_N = 3(X_\pi^2/X_N^2)|^*$ then the lines would go exactly through the physical point. Also this means from the discussion in section 6 that using other singlet scale choices should lead to a similar result. Secondly, as noted before at the end of section 3, as the expansions have been derived using only

group theoretic arguments, they will be valid for results derived on any lattice volume (though the coefficients of the expansion are still functions of the volume). So here, to test this, we have made separate fits for the two volumes — $24^3 \times 48$ and $32^3 \times 64$. Indeed this shows that finite size effects are present but small.

Thus our present conclusion is that kappa in the range 0.12090 – 0.12095 is within a few percent of the reference κ_0. Most of the results reported here will be at $\kappa_0 = 0.12090$.

8.2 Determination of $\kappa_{0;c}$, α_Z

Although not strictly necessary, we briefly indicate here the determination of $\kappa_{0;c}$, α_Z to illustrate some of the discussion in section 6. Using lowest order χPT (i.e. the fact that the pion mass vanishes if the light quarks vanish) and

$$(am_\pi)^2 \propto am_l + \alpha_Z a\overline{m}\,, \tag{79}$$

where the constant of proportionality from eq. (43) is $2a\alpha = 2aQ_0 = 2aB_0^R Z_m^{NS}$, we first determine $\kappa_{0;c}$ (the critical hopping parameter on the flavour symmetric line) as defined in eq. (64). In Fig. 12 we show the plot of $(am_\pi)^2$ versus $1/\kappa_l$

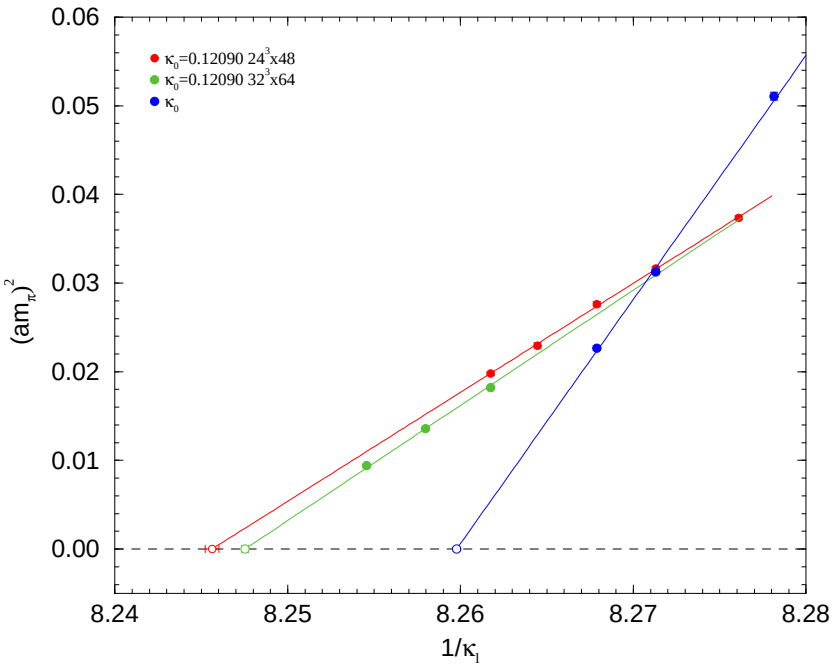

Figure 12: $(am_\pi)^2$ versus $1/\kappa_l$ for both the flavour symmetric case (blue points) and for the $\kappa_0 = 0.12090$ case.

together with linear fits. From the blue points we find

$$\frac{1}{\kappa_{0;c}} = 8.25977(21)\,, \qquad \text{or} \quad \kappa_{0;c} = 0.121069(25)\,, \tag{80}$$

which is in good agreement with the Schrödinger functional determination, see Appendix D. This gives in turn for $\kappa_0 = 0.12090$,

$$a\overline{m} = \frac{1}{2}\left(\frac{1}{\kappa_0} - \frac{1}{\kappa_{0;c}}\right) = 0.00576(21)\,. \tag{81}$$

Note that for $\kappa_l < \kappa_{0;c}$ then the bare am_q is negative (but the renormalised m_q^R is always positive).

α_Z can then be estimated using the $\overline{m} = $ const. line as here $(am_{ps})^2$ vanishes at κ_c, giving

$$\alpha_Z = -\frac{am_q|_{\kappa=\kappa_c}}{a\overline{m}} = \frac{\left(\frac{1}{\kappa_{0;c}} - \frac{1}{\kappa_c}\right)}{\left(\frac{1}{\kappa_0} - \frac{1}{\kappa_{0;c}}\right)}\,. \tag{82}$$

Using the $32^3 \times 64$ data only (green points) gives

$$\frac{1}{\kappa_c} = 8.24753(19)\,, \qquad \text{or} \quad \kappa_c = 0.121248(23)\,. \tag{83}$$

Hence this gives here

$$\alpha_Z = \frac{0.01224(28)}{0.01153(21)} = 1.062(31)\,. \tag{84}$$

Note that the determination is quite sensitive to small changes in $\kappa_{0;c}$ and κ_c. We conclude that for clover fermions at present day lattice spacings α_Z is substantial $\sim O(1)$.

8.3 Singlet quantities and the scale

We take Fig. 11 as a sign that singlet quantities are very flat and the fluctuations are due to low statistics. We now investigate this further. In Fig. 13 we show aX_S for $S = \Delta$, N, ρ and π against M_π^2/X_π^2 for $\kappa_0 = 0.12090$, 0.12092, together with constant fits. This indicates that other singlet quantities are also rather flat (we interpret variations in X_Δ to be due statistical fluctuations). Again fits are made for each lattice volume separately.

8.3.1 Finite size effects

In Fig. 13 there are again indications of relatively small finite size effects. We now briefly investigate this a little more. While we do not attempt to formally derive a formula here, we do have the obvious constraint that the finite size X_S must also be flat at the symmetry point. Thus from eq. (32) and as we shall consider only the lowest order term from eq. (38), we expect the finite size functional form to be

$$X_S(L) = X_S\left(1 + c_S\tfrac{1}{3}[f_L(M_\pi) + 2f_L(M_K)]\right)\,, \tag{85}$$

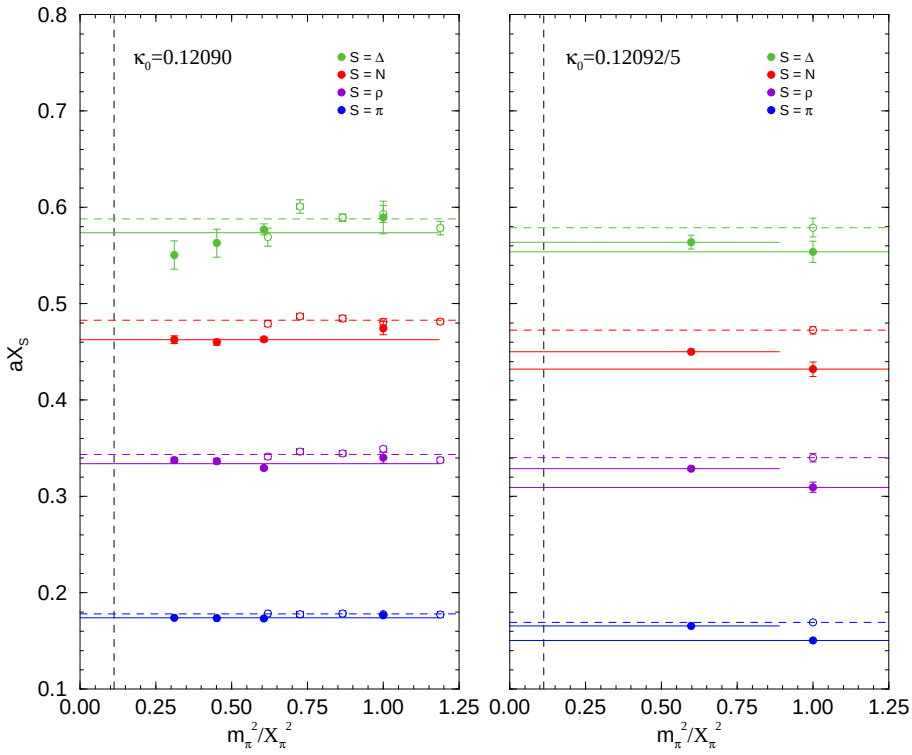

Figure 13: aX_S for $S = \Delta$, N, ρ and π versus M_π^2/X_π^2 for $\kappa_0 = 0.12090$ (left panel) and 0.12092, 0.12095 (right panel) together with constant fits. Filled points and lines are for $32^3 \times 64$ lattices, while opaque points and dashed lines are for $24^3 \times 48$ lattices. In the right panel the *lower* filled points and lines are for $\kappa_0 = 0.12095$.

To lowest order χPT indicates that a suitable form for $f_L(M)$ is

$$f_L(M) = (aM)^2 \frac{e^{-ML}}{(ML)^{\frac{3}{2}}} \,. \tag{86}$$

In Fig. 14 we plot $(f_L(M_\pi) + 2f_L(M_K))/3$ against aX_S for $S = \Delta$, N, ρ, π and r on $32^3 \times 64$, $24^3 \times 48$ and $16^3 \times 32$ lattices for $\kappa_0 = 0.12090$. The fits are linear. A reasonable agreement is seen. (The noisiest signal is for $S = \Delta$.) We see that the extrapolated (i.e. $L \to \infty$) results are very close to the largest lattice results (i.e. $32^3 \times 64$), so we conclude that using the largest lattice size available should only introduce small errors. We shall also go a little further and assume that finite size effects for masses are similar to those of X_S for each mass of the appropriate multiplet. Thus we shall later consider ratios M/X_S for all the available lattice data; finite size results then tend to cancel in the ratio.

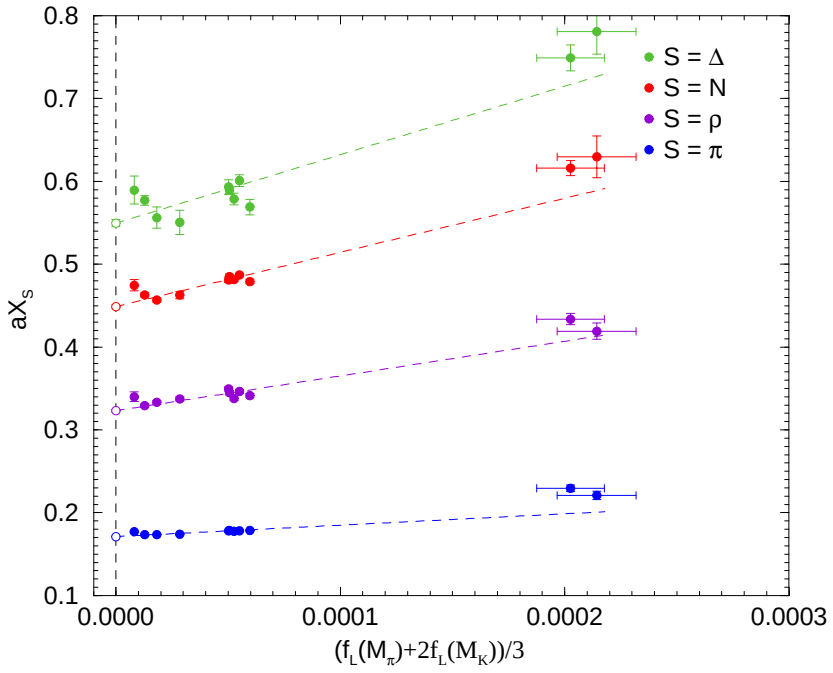

Figure 14: aX_S versus $(f_L(M_\pi) + 2f_L(M_K))/3$ for $\kappa_0 = 0.12090$, with $S = \Delta$, N, ρ, π and r. The left-most clusters of points are from the $32^3 \times 64$ lattices ($L = 32a$), then follow $24^3 \times 48$ and finally $16^3 \times 32$ lattices. The dashed lines are linear fits.

8.3.2 Scale estimation

The result of section 8.3.1 is that the largest volumes available seem to have small finite size effects, so we now simply take the largest volume available. In Fig. 15 we plot $aX_S/X_S \equiv (aX_S)^{lat}/X_S^{phys}$, for $S = N$, Δ, ρ, π using the largest volume fitted results from Fig. 13 (together with smaller data sets for $\kappa_0 = 0.12080$, $\kappa_0 = 0.12095$). This ratio gives estimates for the lattice spacing a for the various scales. We expect convergence to a common scale where the lines cross, assuming all $O(a^2)$ corrections are negligible. We would expect most variation of the ratio with X_π. This appears to be the case, with the exception of the decuplet scale. However this is the channel with the worst signal, so presently we just consider the approximate crossing of the other lines giving $a \sim 0.075 - 0.078\,\text{fm}$ with $\kappa_0 \approx 0.12092$.

As discussed in section 8.3.1 we expect a (partial) cancellation of finite size effects (and also statistical fluctuations) within the same multiplet so we shall adopt the philosophy when considering the hadron spectrum of first finding the ratio of the mass to the singlet quantity from the same multiplet. For example, we can take as our base singlet quantity the baryon octet X_N (not only are these stable particles under QCD interactions and so might physically be considered a

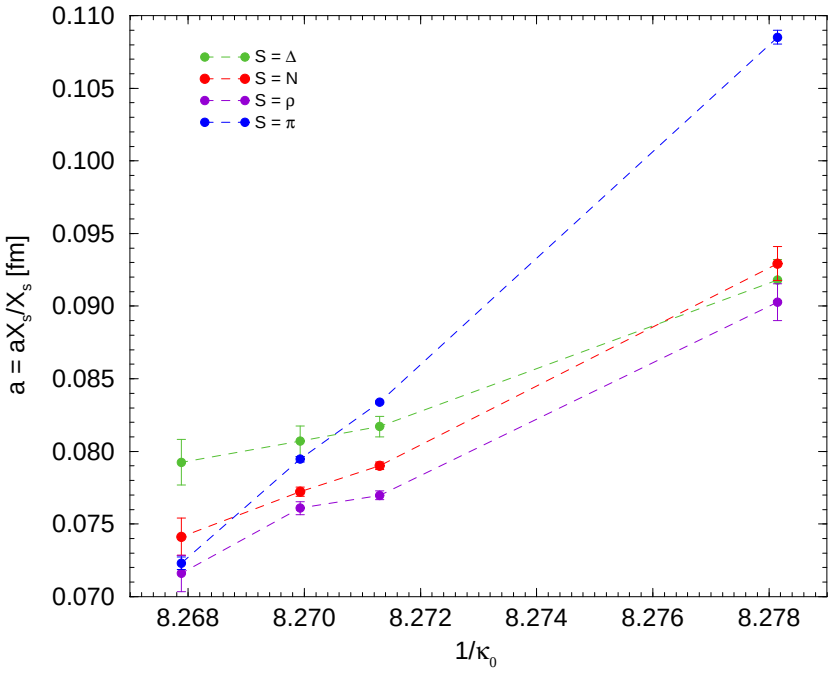

Figure 15: aX_S/X_S against $1/\kappa_0$ for $S = N$, Δ, ρ, π and $\kappa_0 = 0.12080$, 0.12090, 0.12092 and 0.12095.

good choice, but X_N also has smaller numerical errors than X_Δ). To translate from one scale to another we then need the ratio X_S/X_N. In Fig. 16 we plot X_S/X_N for various X_S (with $S = \Delta$, ρ, π). Also shown are constant fits to the two volumes — $24^3 \times 48$ and $32^3 \times 64$. The change in the ratios between the two volumes is seen to be small. Note also that all ratios are close to their physical values. We use the results of the largest volume, which are given in Table 10. In the last column of this table we have used the experimental values of X_S (as

Ratio	$\kappa_0 = 0.12090$	$\times X_N/X_S$
aX_π/aX_N	0.3766(13)	1.054(4)
aX_ρ/aX_N	0.7211(37)	0.972(5)
aX_Δ/aX_N	1.2350(110)	1.030(10)

Table 10: Lattice ratios of singlet quantities aX_S/aX_N, $S = \pi$, ρ, Δ from $32^3 \times 64$ lattices. In the last column we have multiplied by the experimental inverse ratio, taken from Table 11.

given in Table 11) to form the ratio $aX_S/aX_N \times X_N/X_S$. This should be one. As can be seen from Fig. 16, this is the case and Table 10 confirms that the ratios

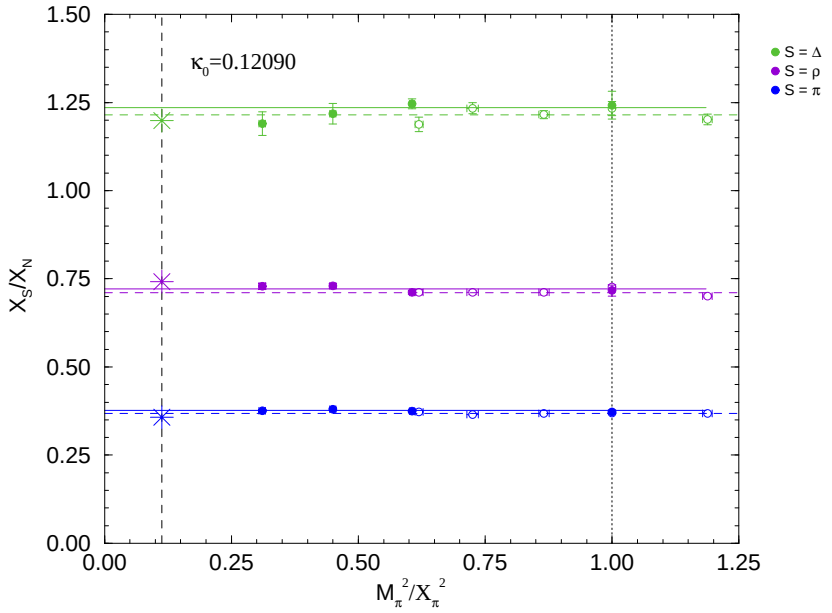

Figure 16: X_S/X_N versus M_π^2/X_π^2 for $S = N$, Δ and ρ for $\kappa_0 = 0.12090$. The dashed vertical line represents the physical value, while the dotted line gives the $SU(3)$ flavour symmetric point. Filled points are on $32^3 \times 64$ lattices while open points are on $24^3 \times 48$ sized lattice. Dashed horizontal lines represent constant fits to either the $32^3 \times 64$ or $24^3 \times 48$ results. For illustration, we also show physical values – denoted by stars.

are one within a few percent.

9 Spectrum results for $n_f = 2 + 1$ flavours

9.1 Experimental values

To minimise u–d quark mass differences (and also electromagnetic effects) for the experimental data, we average the particle masses as given in the Particle Data Group tables [29] over isospin I_3 (i.e. horizontally in Figs. 2, 3). This gives the experimental values (which we give later together with the measured lattice values) in Table 12. Using these experimental numbers, the experimental values for the hadron singlet quantities used here are then given in Table 11.

9.2 Mass hierarchy

We now consider the lattice results for the mass spectrum. First we check whether there is a strong hierarchy due to the $SU(3)$ flavour symmetry as found in eq. (33). In Fig. 17 we plot $(4M_\Delta + 3m_{\Sigma^*} + 2M_{\Xi^*} + M_\Omega)/X_\Delta$, $(-2M_\Delta + M_{\Xi^*} + M_\Omega)/X_\Delta$,

Singlet	GeV
$X_\pi = \sqrt{(M_\pi^2 + 2M_K^2)/3}$	0.4109
$X_\rho = (M_\rho + 2M_K)/3$	0.8530
$X_N = (M_N + M_\Sigma + M_\Xi)/3$	1.1501
$X_\Delta = (2M_\Delta + M_\Omega)/3$	1.3788

Table 11: Experimental values for the X_S singlet quantities, $S = \pi$, N, Δ.

$(4M_\Delta - 5M_{\Sigma^*} - 2M_{\Xi^*} + M_\Omega)/X_\Delta$ and $(-M_\Delta + 3M_{\Sigma^*} - 3M_{\Xi^*} + M_\Omega)/X_\Delta$ against M_π^2/X_π^2 for $\kappa_0 = 0.12090$. Also shown are the experimental values. There is reasonable agreement with these numbers. Well reproduced, as expected, is the order of magnitude drop in the hadron mass contributions with each additional power of δm_l. (See [28] for a similar investigation of octet baryons.) It is also seen that while $(-2M_\Delta + M_{\Xi^*} + M_\Omega)/X_\Delta$ has a linear gradient in the pion mass, in the other fits any gradient is negligible as expected. To check for possible finite size effects we also plot a run at the same (κ_l, κ_s) but using $24^3 \times 48$ lattice rather than $32^3 \times 64$. There is little difference and so it appears that considering ratios of quantities within the same multiplet leads to (effective) cancellation of finite size effects.

9.3 'Fan' plots

We now show a series of plots of the hadron masses from a light quark mass just above the flavour symmetric line down to the physical point. As the masses (of a particular octet or decuplet) are all degenerate from a point on the flavour symmetric line, then we would expect a 'fanning' out of masses from this point. We consider second order fits in the quark mass, but show plots using the pseudoscalar mass on the x-axis, i.e. from eq. (34). Thus we are using the quark mass as an 'internal parameter'.

In Fig. 18 we show $M_{\pi_O}^2/X_\pi^2$ ($\pi_O = \pi$, K, η_s) against M_π^2/X_π^2 together with the combined fit. A typical 'fan' structure is seen with results radiating from the common point on the symmetric line. Note that one point has a light strange quark and a heavy 'light' quark. There is however little real content in this plot – the $\pi_O = \pi$ line is trivial, for the $\pi_O = K$ line the chiral limit and gradient are known. However the graph does tell us that for the fictitious η_s particle, there is very little curvature, which as this is a constrained fit, must hold for all the pseudoscalar octet particles, including the fictitious one. We also note that ratios within the same multiplet do indeed tend to give cancellation of finite size effects.

In Fig. 19 we plot the vector octet multiplet M_{ρ_O}/X_ρ against M_π^2/X_π^2 for $\rho_O = \rho$, K^*, ϕ_s. Again finite volume effects tend to cancel in the ratio (normalising with the singlet quantity from the same octet) and so both volumes have again been used in the fit. The combined fit uses eqs. (35), (34) again with the bare quark

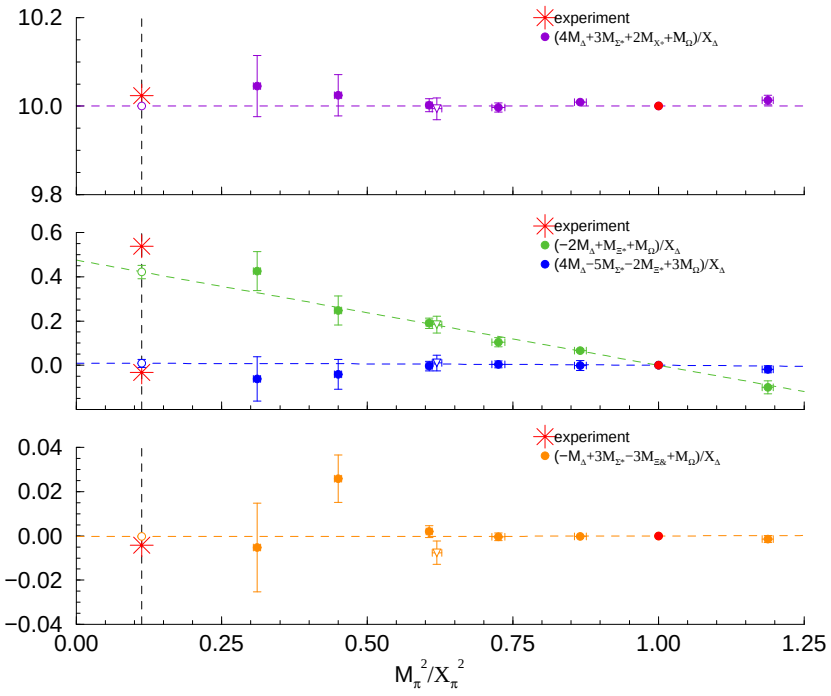

Figure 17: $(4M_\Delta + 3M_{\Sigma^*} + 2M_{\Xi^*} + M_\Omega)/X_\Delta$, $(-2M_\Delta + M_{\Xi^*} + M_\Omega)/X_\Delta$, $(4M_\Delta - 5M_{\Sigma^*} - 2M_{\Xi^*} + M_\Omega)/X_\Delta$ and $(-M_\Delta + 3M_{\Sigma^*} - 3M_{\Xi^*} + M_\Omega)/X_\Delta$ (filled circles) against M_π^2/X_π^2 together with a fit of constant, linear quadratic and cubic term in δm_l respectively. Extrapolated values are shown as opaque circles. Experimental values are denoted by stars. The opaque triangle is a run at the same (κ_l, κ_s), but on a $24^3 \times 48$ lattice rather than a $32^3 \times 64$ lattice.

mass being an 'internal' parameter. Some moderate curvature is now seen in the extrapolations. Note that as $m_{\phi_s} \approx m_\phi$ then we have almost perfect mixing.

Continuing in Fig. 20 we plot the nucleon octet M_{N_O}/X_N (for $N_O = N$, Λ, Σ, Ξ) against M_π^2/X_π^2 and similarly in Fig. 21 we plot the corresponding baryon decuplet M_{Δ_D}/X_Δ for $\Delta_O = \Delta$, Σ^*, Ξ^*, Ω against M_π^2/X_π^2. Although we have included quadratic terms in the fit, there is really very little curvature in the results.

All these figures illustrate the 'fanning' of the results. The correct ordering of the particle spectrum has been achieved (also behind the symmetric point when we have heavy u quark masses and a light s quark mass). The masses (using the scale determined by the appropriate X_S) are given in Table 12. The results are already within a few percent of their experimental values. If we wish to convert these numbers to a base scale, say X_N, then these numbers can be converted

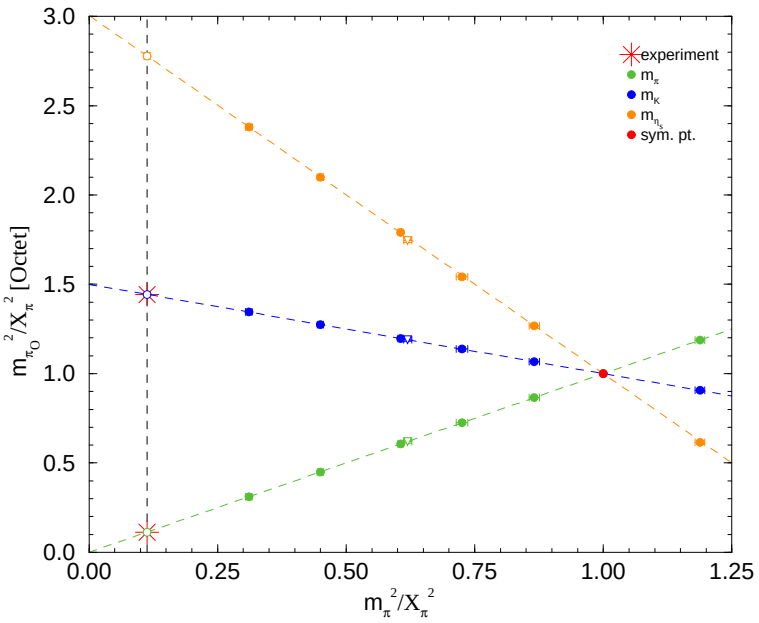

Figure 18: $M^2_{\pi_O}/X^2_\pi$ ($\pi_O = \pi$, K, η_s) against M^2_π/X^2_π together with the combined fit of eq. (34) for both the $32^3 \times 64$ and $24^3 \times 48$ lattices. The flavour symmetric point ('sym. pt.') when $\kappa_0 = 0.12090$ is denoted as a red point. Experimental values are denoted by stars. The opaque triangle is a run at the same mass but on a $24^3 \times 48$ lattice rather than $32^3 \times 64$.

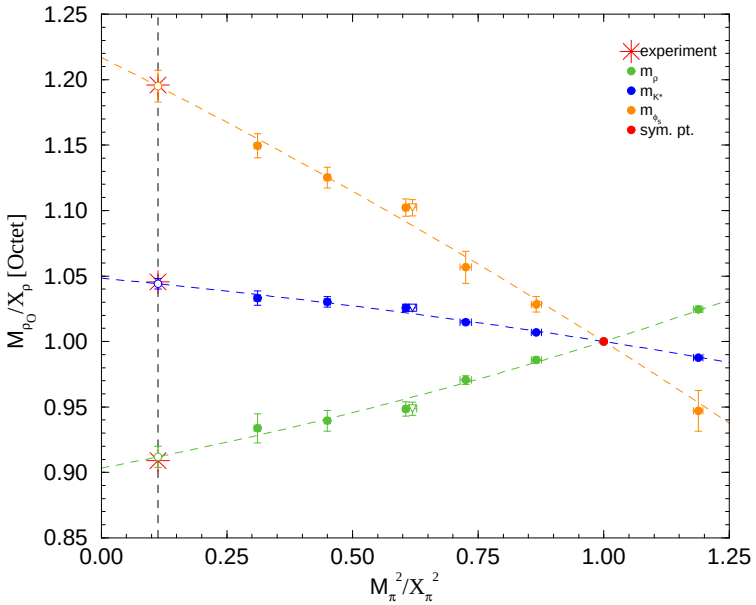

Figure 19: M_{ρ_O}/X_ρ ($\rho_O = \rho$, K^*, ϕ_s) against M^2_π/X^2_π together with the combined fit of eqs. (35), (34) (the dashed lines). Same notation as Fig. 18.

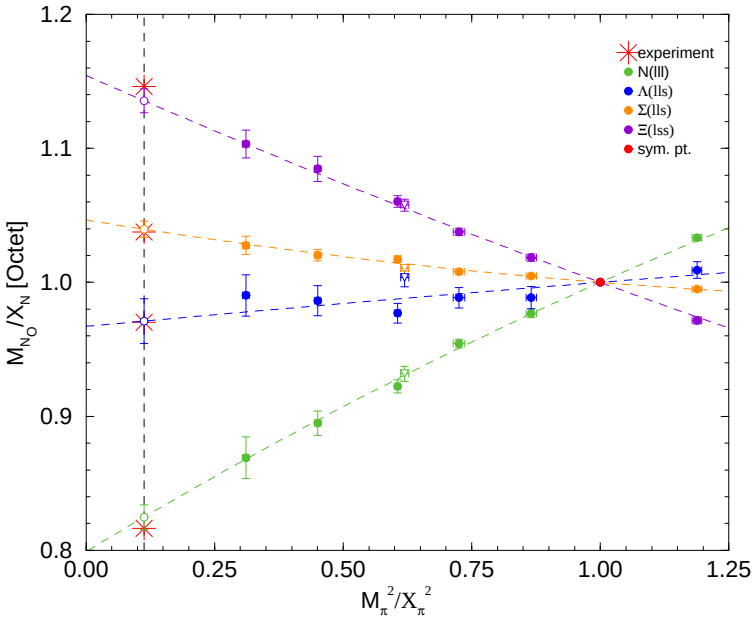

Figure 20: M_{N_O}/X_N ($N_O = N$, Λ, Σ, Ξ) against M_π^2/X_π^2 together with the combined fit of eqs. (36), (34) (the dashed lines). Same notation as Fig. 18.

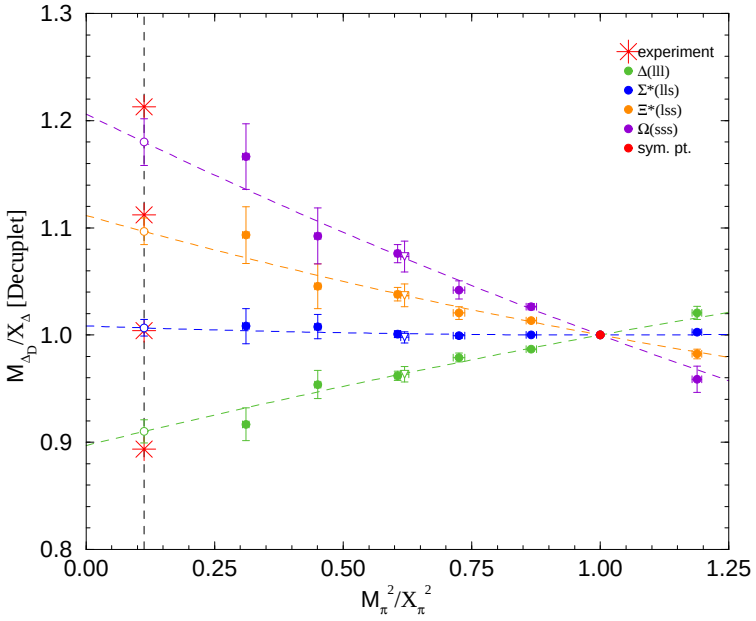

Figure 21: M_{Δ_D}/X_Δ ($\Delta_D = \Delta$, Σ^*, Ξ^*, Ω) against M_π^2/X_π^2 together with the combined fit of eqs. (37), (34). Same notation as Fig. 18.

particle		expt[GeV]	M/X_S	result[GeV]
$M_\pi = (M_{\pi^+} + M_{\pi^0} + M_{\pi^-})/3$	ll	0.1380		
$M_K = (M_{K^+} + M_{K^-})/2$	ls	0.4937		
M_{η_s}	ss		2.778(18)	1.141(7)
$M_\rho = (M_{\rho^+} + M_{\rho^-})/2$	ll	0.7755	0.9119(80)	0.778(7)(22)
$M_{K^*} = (M_{K^{*+}} + M_{K^{*-}})/2$	ls	0.8917	1.044(4)	0.891(3)(25)
$M_{\phi_s} \sim M_\phi$	ss	1.0195	1.195(12)	1.019(10)(29)
$M_N = (M_p + M_n)/2$	lll	0.9389	0.8276(130)	0.952(15)
$M_\Lambda = M_{\Lambda^0}$	lls	1.1157	0.9783(196)	1.125(22)
$M_\Sigma = (M_{\Sigma^+} + M_{\Sigma^0} + M_{\Sigma^-})/3$	lls	1.1932	1.036(12)	1.192(14)
$M_\Xi = (M_{\Xi^0} + M_{\Xi^-})/2$	lss	1.3183	1.137(8)	1.308(9)
M_Δ	lll	1.232	0.9100(108)	1.255(15)(38)
$M_{\Sigma^*} = (M_{\Sigma^{*+}} + M_{\Sigma^{*0}} + M_{\Sigma^{*-}})/3$	lls	1.3846	1.007(8)	1.388(11)(41)
$M_{\Xi^*} = (M_{\Xi^{*0}} + M_{\Xi^{*-}})/2$	lss	1.5334	1.097(12)	1.513(17)(45)
$M_\Omega = M_{\Omega^-}$	sss	1.6725	1.180(22)	1.627(30)(49)

Table 12: The hadron masses. The third column, 'expt', gives the isospin averaged masses. The fourth column, 'results' gives the numerical results from Figs. 18 – 21. The first error is from these fits, while the second is from scale uncertainties as discussed in section 8.3.2 and the text here.

using the numbers in the last column of Table 10 as

$$M_{S_O} = \frac{aM_{S_O}}{aX_N} X_N = \left(\frac{aM_{S_O}}{aX_S} X_S\right) \left(\frac{aX_S}{aX_N} \frac{X_N}{X_S}\right) , \tag{87}$$

where the second factor is given in this table. These numbers are all ~ 1 (within a few percent) and we shall just regard them here as a possible additional source of error (the second error in the last column). It is to be noted that the largest source of error appears to come from the uncertainty, not in the determination of the scale itself, but in the consistency with the use of a different flavour singlet quantity to determine the scale.

9.4 Partially quenched results

We illustrate partially quenching using baryon splittings as an example. The splittings depend mainly on $m_s^{val} - m_l^{val}$ and only weakly (at second order) on other quark combinations. In the PQ data shown here, we have points with a large splitting between m_s and m_l reaching up to points where $m_s - m_l$ is equal to its physical value. We can therefore make partially quenched splitting plots reaching down to the physical point.

We have generated partially quenched results on an ensemble with $\kappa_0 = 0.12090$ and lattice volume $24^3 \times 48$. The first octet splitting diagram, Fig. 22, shows just the PQ data. The second, Fig. 23, shows the PQ data in grey,

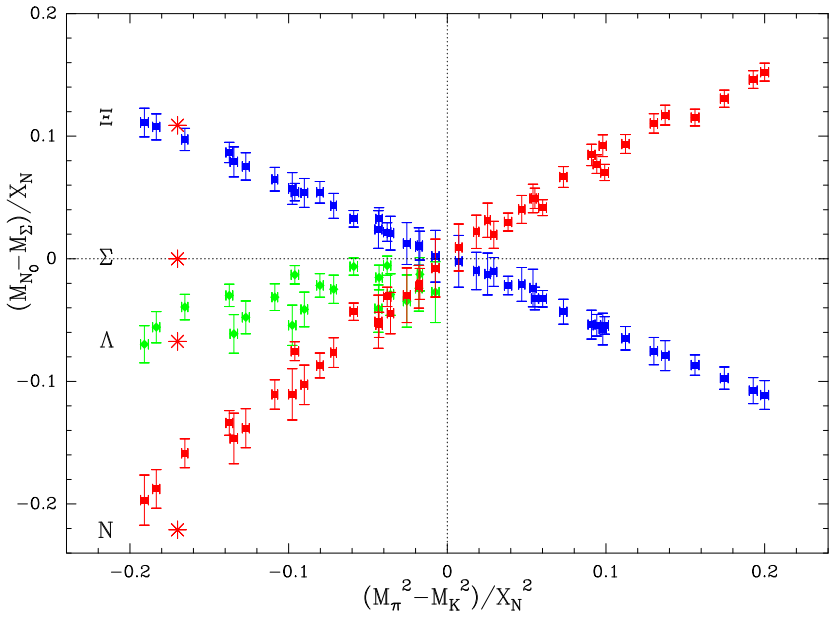

Figure 22: Partially quenched data, $(M_{NO} - M_\Sigma)/X_N$ versus $(M_\pi^2 - M_K^2)/X_N^2$. The experimental points are denoted by a red stars.

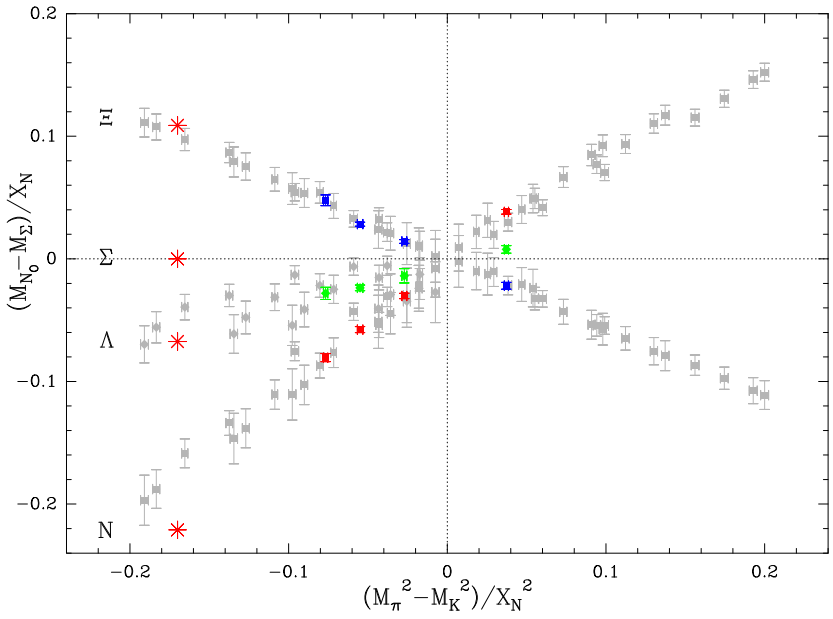

Figure 23: A comparison between partially quenched and full data from $24^3 \times 48$ lattices, $(M_{NO} - M_\Sigma)/X_N$ versus $(M_\pi^2 - M_K^2)/X_N^2$. Same notation as in Fig.22.

compared with the $24^3 \times 48$ data in colour. While only to be taken as an an illustration, it shows that the PQ data has the potential to be a good predictor of real data.

10 Conclusions

We have outlined a programme to systematically approach the physical point starting from a point on the $SU(3)$ flavour symmetric line by keeping the singlet quark mass constant. This leads to highly constrained extrapolations (i.e. fits). Exploratory results for the hadron mass spectrum show that indeed this occurs, with all fits for the pseudoscalar, vector and baryon octets and baryon decuplet being highly linear. This is also seen when considering flavour singlet quantities, which remain constant as we approach the physical point. This enables the lattice spacing to be determined, and indeed allows the consistency of various definitions to be discussed. We have also extended these results to the partially quenched case and illustrated that they contain useful information. (We plan to discuss this further in [17].) We are also applying this method to the computation of matrix elements, some initial results are given in [32, 33].

Acknowledgements

The numerical calculations have been performed on the IBM BlueGeneL at EPCC (Edinburgh, UK), the BlueGeneL and P at NIC (Jülich, Germany), the SGI ICE 8200 at HLRN (Berlin-Hannover, Germany) and the JSCC (Moscow, Russia). We thank all institutions. The BlueGene codes were optimised using Bagel, [34]. This work has been supported in part by the EU grants 227431 (Hadron Physics2), 238353 (ITN STRONGnet) and by the DFG under contract SFB/TR 55 (Hadron Physics from Lattice QCD). JZ is supported by STFC grant ST/F009658/1.

Appendix

A The permutation group S_3

If we have three quarks u, d, s with different masses, physics should be unchanged if we simply permute the names we give to the quarks. The permutation group is not the complete symmetry group - for example we could also perform $U(1)$ phase rotations on any particular quark flavour – but it is already enough to tell us something useful.

The permutation group of 3 objects, S_3, is the same as the symmetry group of an equilateral triangle, C_{3v}. There are 6 group operations

1. The identity
$$u \to u\,,\ d \to d\,,\ s \to s\,. \tag{88}$$
2. Two cyclic permutations
$$u \to d\,,\ d \to s\,,\ s \to u \qquad \text{and} \qquad u \to s\,,\ s \to d\,,\ d \to u\,, \tag{89}$$
which correspond to rotations of the triangle through $\pm 120^{\rm o}$, and rotations of the (I_3, Y) diagram through $\pm 120^{\rm o}$.
3. Three pair interchanges
$$u \leftrightarrow d\,,\ s \to s; \qquad u \leftrightarrow s\,,\ d \to d; \qquad d \leftrightarrow s\,,\ u \to u\,, \tag{90}$$
which correspond to the 3 reflection symmetries of the triangle, and reflections in the I_3–Y plane.

If an equation is to respect flavour blindness, both sides of the equation should transform the same way under all 6 operations. The representations of the group allow us to arrange for this to hold.

The permutation group S_3 is a subgroup of $SU(3)$ and has 3 irreducible representations [6], two different singlets, A_1 and A_2; and a doublet E.

A.1 Singlet representation A_1

The representation A_1 includes objects which are invariant under all 6 group operations. Examples include gluonic quantities, such as glueball masses, r_0, $V(r), \ldots$ as well as certain averages over hadron multiplets. (We shall collectively denote these objects by X.) A_1 is a singlet representation. Examples of quark masses with A_1 symmetry (complete up to $O(m_q^3)$) are

$$\begin{array}{l} 1 \\ m_u + m_d + m_s \\ (m_u + m_d + m_s)^2\,, \quad m_u^2 + m_d^2 + m_s^2 \\ (m_u + m_d + m_s)^3\,, \quad (m_u + m_d + m_s)(m_u^2 + m_d^2 + m_s^2)\,, \quad m_u^3 + m_d^3 + m_s^3 \end{array} \tag{91}$$

and linear combinations of these.

A.2 Singlet representation $\mathbf{A_2}$

This consists of objects which are invariant under the cyclic quark permutations, (triangle rotations), but which change sign under the pair exchanges, (reflections). A_2 quantities automatically vanish if any two quark masses are the same. The lowest A_2 quantity for quark masses is $O(m_q^3)$,

$$\begin{aligned} & m_u m_s^2 - m_d m_s^2 + m_d^2 m_s - m_u^2 m_s + m_u^2 m_d - m_d^2 m_u \\ = \;& (\delta m_s - \delta m_u)(\delta m_s - \delta m_d)(\delta m_u - \delta m_d)\,. \end{aligned} \tag{92}$$

Baryon mass combinations with A_2 symmetry are

$$M_p - M_n + M_{\Sigma^-} - M_{\Sigma^+} + M_{\Xi^0} - M_{\Xi^-}\,, \tag{93}$$

and the corresponding decuplet quantity, with the p and n replaced by Δ^+ and Δ^0. Because particle and antiparticle have the same mass, the mesonic analogue of eq. (93) vanishes.

Group theory tells us that in a $1+1+1$ flavour world, the splitting eq. (93) would be proportional to eq. (92) and terms of even higher order in m_q (neglecting electromagnetic effects).

A.3 Doublet representation E

By considering A_2 we have found a fairly useless mass splitting formula, but by looking at the doublet E we are able to find some more useful formulae.

The E representation has two states, which mix under the cyclic permutations. We can choose to make one state of the doublet even under the reflection $u \leftrightarrow d$, and the other state odd. (We could just as well choose any interchange to classify our states, but it makes best sense to choose $u \leftrightarrow d$, because the hadronic universe is almost invariant under that operation.) We have called the even member of the doublet E^+, the odd member E^-. (There does not appear to be a standard notation.)

An example of an E doublet would be the states

$$\frac{1}{\sqrt{6}}\left(2|s\rangle - |u\rangle - |d\rangle\right) \qquad \text{and} \qquad \frac{1}{\sqrt{2}}\left(|u\rangle - |d\rangle\right)\,, \tag{94}$$

It is easily checked that under any group operation they just mix with each other, for example under the cyclic operation $u \to d$, $d \to s$, $s \to u$:

$$\begin{aligned} \frac{1}{\sqrt{6}}\left(2|s\rangle - |u\rangle - |d\rangle\right) \;&\to\; \frac{1}{\sqrt{6}}\left(2|u\rangle - |d\rangle - |s\rangle\right) \\ &= \frac{\sqrt{3}}{2}\,\frac{1}{\sqrt{2}}\left(|u\rangle - |d\rangle\right) - \frac{1}{2}\,\frac{1}{\sqrt{6}}\left(2|s\rangle - |u\rangle - |d\rangle\right) \end{aligned} \tag{95}$$

and so on. In other words, the matrix for a cyclic permutation has the form

$$R = \begin{pmatrix} \cos\theta & \mp\sin\theta \\ \pm\sin\theta & \cos\theta \end{pmatrix} \tag{96}$$

with $\theta = 120^{\rm o}$.

Quark mass terms with E doublet symmetry are

$$\begin{array}{l}
\left\{ \frac{1}{\sqrt{6}}(2m_s - m_u - m_d) \quad , \quad \frac{1}{\sqrt{2}}(m_u - m_d) \right\} \\
\left\{ \frac{1}{\sqrt{6}}(2m_s^2 - m_u^2 - m_d^2) \quad , \quad \frac{1}{\sqrt{2}}(m_u^2 - m_d^2) \right\} \\
\left\{ \frac{1}{\sqrt{6}}(m_u m_s + m_d m_s - 2m_u m_d) \quad , \quad \frac{1}{\sqrt{2}}(m_u m_s - m_d m_s) \right\} \\
\left\{ \frac{1}{\sqrt{6}}(2m_s^3 - m_u^3 - m_d^3) \quad , \quad \frac{1}{\sqrt{2}}(m_u^3 - m_d^3) \right\} \\
\left\{ \frac{1}{2}(m_u m_s^2 + m_d m_s^2 - m_u^2 m_d - m_u m_d^2) \quad , \right. \\
\qquad \left. \frac{1}{\sqrt{12}}(m_u m_s^2 + m_d m_s^2 + 2m_u^2 m_s - 2m_d^2 m_s + m_u^2 m_d + m_u m_d^2) \right\} \\
\left\{ \frac{1}{\sqrt{12}}(m_u m_s^2 + m_d m_s^2 - 2m_u^2 m_s - 2m_d^2 m_s + m_u^2 m_d + m_u m_d^2) \right. \\
\qquad \left. , \quad \frac{1}{2}(-m_u m_s^2 + m_d m_s^2 + m_u^2 m_d - m_u m_d^2) \right\}
\end{array} \tag{97}$$

The normalisations and phases have been chosen so that each pair transforms in the same way as eq. (94) under all group operations i.e. the matrices which represent the group operations are the same for every pair.

B Some group theory

If the three quarks have equal masses, the QCD Lagrangian is invariant under a global $U(1)$ transformation of the quark fields

$$\psi \to e^{i\theta}\psi\,, \qquad \overline{\psi} \to \overline{\psi} e^{-i\theta}\,, \tag{98}$$

(corresponding to baryon number conservation) and a global $SU(3)$ flavour transformation

$$\psi \to U\psi\,, \qquad \overline{\psi} \to \overline{\psi} U^\dagger\,, \tag{99}$$

with U a unitary matrix with determinant 1.

If the quarks are all given different masses we still have the freedom to change the phase of each flavour separately, without changing the action, so we have conserved currents for each of the three flavours, and three independent $U(1)$ symmetries.

When the quarks have different masses, flavour $SU(3)$ is no longer a symmetry of the action, a global $SU(3)$ rotation no longer leaves the action unchanged, but we can still use $SU(3)$ to understand the action. Consider the transformation

$$\mathcal{M} \to U\mathcal{M}U^\dagger \equiv \mathcal{M}' \tag{100}$$

(the flavour analogue of a global gauge rotation in colour). If the quarks have different masses, $\mathcal{M}' \neq \mathcal{M}$, but they are physically equivalent in the sense that the two matrices have the same eigenvalues as each other, but the eigenvectors are rotated

$$\psi' = U\psi, \qquad \overline{\psi}' = \overline{\psi}U^\dagger \,. \tag{101}$$

B.1 Flavour permutations, S_3, as a subgroup of SU(3)

We want to concentrate initially on a set of $SU(3)$ matrices which map a diagonal mass matrix to another diagonal matrix when used in eq.(100). These are

- the identity matrix,

$$I = \begin{pmatrix} 1 & 0 & 0 \\ 0 & 1 & 0 \\ 0 & 0 & 1 \end{pmatrix} \tag{102}$$

- the cyclic permutations of the quark flavours,

$$\begin{aligned} \begin{pmatrix} 0 & 0 & 1 \\ 1 & 0 & 0 \\ 0 & 1 & 0 \end{pmatrix} &= \exp\left\{ i\,\frac{2\pi}{3\sqrt{3}} \begin{pmatrix} 0 & i & -i \\ -i & 0 & i \\ i & -i & 0 \end{pmatrix} \right\} \\ \begin{pmatrix} 0 & 1 & 0 \\ 0 & 0 & 1 \\ 1 & 0 & 0 \end{pmatrix} &= \exp\left\{ -i\,\frac{2\pi}{3\sqrt{3}} \begin{pmatrix} 0 & i & -i \\ -i & 0 & i \\ i & -i & 0 \end{pmatrix} \right\} \end{aligned} \tag{103}$$

- pair interchanges,

$$\begin{aligned} \begin{pmatrix} 0 & -1 & 0 \\ -1 & 0 & 0 \\ 0 & 0 & -1 \end{pmatrix} &= \exp\left\{ i\,\frac{\pi}{2} \begin{pmatrix} 1 & 1 & 0 \\ 1 & 1 & 0 \\ 0 & 0 & -2 \end{pmatrix} \right\} \\ \begin{pmatrix} 0 & 0 & -1 \\ 0 & -1 & 0 \\ -1 & 0 & 0 \end{pmatrix} &= \exp\left\{ i\,\frac{\pi}{2} \begin{pmatrix} 1 & 0 & 1 \\ 0 & -2 & 0 \\ 1 & 0 & 1 \end{pmatrix} \right\} \\ \begin{pmatrix} -1 & 0 & 0 \\ 0 & 0 & -1 \\ 0 & -1 & 0 \end{pmatrix} &= \exp\left\{ i\,\frac{\pi}{2} \begin{pmatrix} -2 & 0 & 0 \\ 0 & 1 & 1 \\ 0 & 1 & 1 \end{pmatrix} \right\} \end{aligned} \tag{104}$$

Note that when we interchange a quark pair, we also have to change the sign of the quarks, to keep the determinant equal to 1, as required for a matrix in $SU(3)$. These six matrices are all unitary with determinant 1, so they are all members of $SU(3)$. We have also shown that all the matrices can be written in the canonical $SU(3)$ form $\exp\{i\sum \alpha_j \lambda_j\}$. These matrices form a closed set under multiplication, with a multiplication table matching that of the group S_3, showing that the symmetries of the equilateral triangle are a subgroup of $SU(3)$.

B.2 Group classification of quark mass polynomials

This subsection explains how the final column of Table 3 was calculated.

We can establish many useful results from the S_3 subgroup, but it has its limitations, it does not connect particles in different permutation sets, see Fig. 4. By considering S_3 alone we cannot write down a formula for the mass difference between the Σ^0 and Σ^-, we cannot even show that the two particles have the same mass in the $2+1$ case. To go further we need to consider the full $SU(3)$ group, even though this will involve operations which make the mass matrix non-diagonal.

We can write any $SU(3)$ rotation as a matrix of the form

$$U = \exp\left\{ i \sum_{j=1}^{8} \alpha_j \lambda_j \right\} , \tag{105}$$

where the λ_j are the 8 Gell-Man matrices (and α_j are real parameters). We only need to consider infinitesimal transformations

$$\mathcal{M} \to U\mathcal{M}U^\dagger = \mathcal{M} + i\sum_{j=1}^{8} \alpha_j \left(\lambda_j \mathcal{M} - \mathcal{M}\lambda_j\right) = \mathcal{M} + i\sum_{j=1}^{8} \alpha_j \left[\lambda_j, \mathcal{M}\right] . \tag{106}$$

We write

$$\begin{aligned} \mathcal{O}_j \psi &= \lambda_j \psi \\ \mathcal{O}_j \overline{\psi} &= -\overline{\psi}\lambda_j \\ \mathcal{O}_j \mathcal{M} &= \left[\lambda_j, \mathcal{M}\right] , \end{aligned} \tag{107}$$

to represent the action of the eight generators of $SU(3)$ on spinors and on matrices. The eight operators $\mathcal{O}_j$ are analogous to the three operators J_j in angular momentum.

In $SU(2)$ we use the eigenvalues of the operator

$$J^2 = \sum_{j=1}^{3} J_j^2 , \tag{108}$$

to identify the irreducible representations of angular momentum. Similarly in $SU(3)$ we can use the eigenvalues of the quadratic Casimir operator [12, 13]

$$\mathcal{C} = \frac{1}{4}\sum_{j=1}^{8} \mathcal{O}_j^2 , \tag{109}$$

to identify irreducible representations of $SU(3)$. (The factor $\frac{1}{4}$ is a conventional normalisation.) Acting on a matrix

$$\mathcal{C}\mathcal{M} = \frac{1}{4}\sum_{j=1}^{8} \left[\lambda_j, \left[\lambda_j, \mathcal{M}\right]\right] = \frac{1}{4}\sum_{j=1}^{8} \left(\lambda_j^2 \mathcal{M} - 2\lambda_j \mathcal{M} \lambda_j + \mathcal{M}\lambda_j^2\right) . \tag{110}$$

We can now begin classifying polynomial functions of $\mathcal{M}$. At first order, linear functions of mass, it is simple,

$$\mathrm{Tr}[\mathcal{M}] = \mathcal{M}_{11} + \mathcal{M}_{22} + \mathcal{M}_{33}\,, \tag{111}$$

doesn't change under $SU(3)$ transformations, so it is singlet.

The other elements of $\mathcal{M}$ can be assigned quantum numbers. For example $\mathcal{M}_{21}$ takes a u quark and changes it to a d, so it has $I_3 = -1$ and hypercharge 0. The 6 off-diagonal elements of $\mathcal{M}$ form the outer ring of the octet. The two central elements of the octet are the combinations

$$\begin{aligned} 2\mathcal{M}_{33} - \mathcal{M}_{11} - \mathcal{M}_{22} &\propto \mathrm{Tr}[\lambda_8\mathcal{M}] \\ \mathcal{M}_{11} - \mathcal{M}_{22} &\propto \mathrm{Tr}[\lambda_3\mathcal{M}]\,. \end{aligned} \tag{112}$$

We can check that both are eigenstates of the Casimir operator, with eigenvalue 3, showing that both are pure octet quantities.

If we make the substitutions

$$\mathcal{M}_{11} \to m_u\,, \quad \mathcal{M}_{22} \to m_d\,, \quad \mathcal{M}_{33} \to m_s\,, \tag{113}$$

we see that the quantities eqs. (111)–(112) are proportional to the three linear polynomials in Table 3, with the $SU(3)$ assignments given from their behaviour when operated on by the Casimir operator.

It gets more interesting at second order. $(\mathrm{Tr}[\mathcal{M}])^2$ and $\mathrm{Tr}[\mathcal{M}^2]$ are both flavour-singlet functions of the mass matrix. It is more convenient to work with the linear combinations

$$\begin{aligned} &(\mathrm{Tr}[\mathcal{M}])^2 \\ &3\mathrm{Tr}[\mathcal{M}^2] - (\mathrm{Tr}[\mathcal{M}])^2\,, \end{aligned} \tag{114}$$

where we have chosen the coefficients so that the second combination will be zero at the $SU(3)$ symmetric point. At second order we should be able to construct functions of the mass matrix that are in the 1, 8 and 27 representations. One way of constructing a quantity that is purely 27-plet is by using the Casimir operator. If we take an arbitrary quadratic function of $\mathcal{M}$ it will usually be a mixture of all three representations. If we multiply by

$$(\mathcal{C} - 3)\mathcal{C}\,, \tag{115}$$

$\mathcal{C}$ will cancel the singlet part, $(\mathcal{C} - 3)$ will kill the octet part, (see Table 13), so the operator eq. (115) leaves a pure 27-plet function of $\mathcal{M}$. Using the eigenvalues in Table 13 we can construct similar operators to project out objects in the other representations of $SU(3)$. Of course it would be tedious to do this by hand: we have programmed the group operations in Mathematica so that the group theory can be done more easily and rapidly.

Representation	1	8	10	$\overline{10}$	27	64
Casimir eigenvalue	0	3	6	6	8	15

Table 13: The eigenvalues of the quadratic Casimir operator, $\mathcal{C}$, eq. (109), for the $SU(3)$ representations needed in this article.

Another useful technique is to use the raising and lowering operators $I_\pm$, $U_\pm$, $V_\pm$ [14] to move around within a multiplet. Once we have one state in a multiplet, these operators allow us to make all the other states. Because infinitesimal $SU(3)$ operations do not preserve diagonality, a typical eigenstate of the Casimir operator will involve all nine elements of the quark mass matrix $\mathcal{M}$, not just the three diagonal elements. For example, if we explicitly write out the $SU(3)$ singlet quantity eq. (114) it is

$$\begin{aligned} P_1 &= 2\mathcal{M}_{11}\mathcal{M}_{11} + 2\mathcal{M}_{22}\mathcal{M}_{22} + 2\mathcal{M}_{33}\mathcal{M}_{33} \\ &\quad +6\mathcal{M}_{12}\mathcal{M}_{21} + 6\mathcal{M}_{13}\mathcal{M}_{31} + 6\mathcal{M}_{23}\mathcal{M}_{32} \\ &\quad -2\mathcal{M}_{11}\mathcal{M}_{22} - 2\mathcal{M}_{11}\mathcal{M}_{33} - 2\mathcal{M}_{22}\mathcal{M}_{33}\,. \end{aligned} \tag{116}$$

We can use the techniques discussed in this section to write down a pure $SU(3)$ 27-plet quantity, with the same S_3 properties as eq. (116); the result is

$$\begin{aligned} P_{27}^{A_1} &= \mathcal{M}_{11}\mathcal{M}_{11} + \mathcal{M}_{22}\mathcal{M}_{22} + \mathcal{M}_{33}\mathcal{M}_{33} \\ &\quad -\mathcal{M}_{12}\mathcal{M}_{21} - \mathcal{M}_{13}\mathcal{M}_{31} - \mathcal{M}_{23}\mathcal{M}_{32} \\ &\quad -\mathcal{M}_{11}\mathcal{M}_{22} - \mathcal{M}_{11}\mathcal{M}_{33} - \mathcal{M}_{22}\mathcal{M}_{33}\,. \end{aligned} \tag{117}$$

Expressed this way, the 27-plet and singlet are clearly different functions of the full 9-element mass matrix. However, if we just consider a diagonal mass matrix, $\mathcal{M}_{ij} = 0$ if $i \neq j$, $\mathcal{M}_{11} = m_u$, $\mathcal{M}_{22} = m_d$, $\mathcal{M}_{33} = m_s$ then the quantities become indistiguishable:

$$\begin{aligned} P_1 &\to 2(m_u^2 + m_d^2 + m_s^2 - m_u m_d - m_u m_s - m_d m_s) = 3(\delta m_u^2 + \delta m_d^2 + \delta m_s^2) \\ P_{27}^{A_1} &\to m_u^2 + m_d^2 + m_s^2 - m_u m_d - m_u m_s - m_d m_s = \frac{3}{2}(\delta m_u^2 + \delta m_d^2 + \delta m_s^2)\,. \end{aligned} \tag{118}$$

Both collapse to the same quark mass polynomial, $\delta m_u^2 + \delta m_d^2 + \delta m_s^2$, so this polynomial is allowed to appear in equations for singlet and 27-plet physical quantities, but not in equations for any other $SU(3)$ representation.

We have used the methods of this subsection to classify all polynomials up to cubic order, the results are recorded in Table 3.

B.3 Group analysis of hadron mass matrices

To construct hadron mass matrices for octet and decuplet hadrons we need to analyse 8×8 and 10×10 matrices by their S_3 and $SU(3)$ properties.

To get started we need to construct 8×8 and 10×10 representations of the $SU(3)$ generators. We can do this by considering the known behaviour of the hadron multiplets under the $SU(2)$ subgroups, isospin I, U-spin and V-spin, and the hypercharge, Y, [14]:

$$\begin{aligned} \lambda_1 &= 2I_1 \qquad \lambda_2 = 2I_2 \qquad \lambda_3 = 2I_3 \\ \lambda_4 &= 2V_1 \qquad \lambda_5 = 2V_2 \\ \lambda_6 &= 2U_1 \qquad \lambda_7 = 2U_2 \\ \lambda_8 &= \sqrt{3}\, Y \end{aligned} \tag{119}$$

These 8×8 or 10×10 λ matrices have the same commutation relations as the usual 3×3 matrices

$$[\lambda_i, \lambda_j] = 2if_{ijk}\lambda_k \,. \tag{120}$$

Once we have the eight λ matrices for our hadron multiplet we can use eq. (110) to classify any other matrices. For the hadron mass matrices, we need all the flavour-conserving matrices. For the decuplet mass matrix these are all diagonal matrices; but for the octet mass matrix they can include some off-diagonal elements, because the Σ^0 and Λ have the same flavour quantum numbers. Our results for the decuplet and octet matrices are given in Tables 4 and 5.

C Coordinate choice for partially quenched formulae

.

It is often convenient to plot quantities against the pseudoscalar meson mass squared, because then we know better the location of the physical point and the chiral limit. If we do want to use pseudoscalar mesons, the best choice is to replace the light sea quark by the full (non partially quenched) pion, the light valence quark by the partially quenched pion, and to replace the valence strange quark mass by the partially quenched $\overline{s}_{val}s_{val}$ meson (the 'strange pion'), which we are calling the η_s. This is a particle that doesn't exist in the real world, but which we can measure in the partially quenched channel. Determining the valence s quark mass from the kaon has disadvantages, as we shall shortly see.

We introduce the mesonic variables

$$\begin{aligned} x \equiv M^2_{\pi^{full}} - M^2_{\pi;0} &= 2\alpha\delta m_l + \beta_0\delta m_l^2 + 2\beta_1\delta m_l^2 \\ y \equiv M^2_{\pi^{PQ}} - M^2_{\pi;0} &= 2\alpha\delta \mu_l + \beta_0\delta m_l^2 + 2\beta_1\delta \mu_l^2 \\ z \equiv M^2_{s} - M^2_{\pi;0} &= 2\alpha\delta \mu_s + \beta_0\delta m_l^2 + 2\beta_1\delta \mu_s^2 \,, \end{aligned} \tag{121}$$

keeping terms up to second order in quark mass. In terms of these variables the decuplet mass formulae eq. (48) become

$$M_\Delta = M_0 + 3\tilde{A}y + \tilde{B}_0x^2 + 3\tilde{B}_1y^2$$

$$
\begin{aligned}
M_{\Sigma^*} &= M_0 + \tilde{A}(2y+z) + \tilde{B}_0 x^2 + \tilde{B}_1(2y^2+z^2) + \tilde{B}_2(z-y)^2 \\
M_{\Xi^*} &= M_0 + \tilde{A}(y+2z) + \tilde{B}_0 x^2 + \tilde{B}_1(y^2+2z^2) + \tilde{B}_2(z-y)^2 \\
M_{\Omega} &= M_0 + 3\tilde{A}z + \tilde{B}_0 x^2 + 3\tilde{B}_1 z^2 \,, \qquad (122)
\end{aligned}
$$

with

$$
\begin{aligned}
\tilde{A} &\equiv \frac{A}{2\alpha} \\
\tilde{B}_0 &\equiv \frac{(2\alpha B_0 - 3A\beta_0)}{8\alpha^3} \\
\tilde{B}_1 &\equiv \frac{(\alpha B_1 - A\beta_1)}{4\alpha^3} \\
\tilde{B}_2 &\equiv \frac{B_2}{4\alpha^2} \,. \qquad (123)
\end{aligned}
$$

The form of eq. (122) exactly repeats the form of eq. (48), but the new constants involve a combination of curvature terms from the pion mass equation and from the baryon mass equation.

Suppose instead we use the PQ kaon mass (instead of the strange pion) to represent the strange quark mass, i.e. we replace z defined in eq.(121) by

$$
\begin{aligned}
w &\equiv 2M^2_{K^{PQ}} - M^2_{\pi^{PQ}} - M^2_{\pi^{full}} \\
&= 2\alpha\delta\mu_s + \beta_0\delta m_l^2 + 2\beta_1\delta\mu_s^2 + 2\beta_2(\delta\mu_s - \delta\mu_l)^2 \,. \qquad (124)
\end{aligned}
$$

At first order, w is just as good as z, but if we are interested in curvature, it is less suitable, because at second order it involves both the valence s and the valence l, unlike eq.(121). Using w instead of z, the decuplet mass formulae become

$$
\begin{aligned}
M_{\Delta} &= M_0 + 3\tilde{A}y + \tilde{B}_0 x^2 + 3\tilde{B}_1 y^2 \\
M_{\Sigma^*} &= M_0 + \tilde{A}(2y+w) + \tilde{B}_0 x^2 + \tilde{B}_1(2y^2+w^2) + \tilde{B}_2(w-y)^2 + \tilde{B}_X(w-y)^2 \\
M_{\Xi^*} &= M_0 + \tilde{A}(y+2w) + \tilde{B}_0 x^2 + \tilde{B}_1(y^2+2w^2) + \tilde{B}_2(w-y)^2 + 2\tilde{B}_X(w-y)^2 \\
M_{\Omega} &= M_0 + 3\tilde{A}w + \tilde{B}_0 x^2 + 3\tilde{B}_1 w^2 + 3\tilde{B}_X(w-y)^2 \,, \qquad (125)
\end{aligned}
$$

with $\tilde{A}, \tilde{B}_0, \tilde{B}_1, \tilde{B}_2$ defined as in eq. (123), but with an extra curvature coefficient

$$
\tilde{B}_X = -\frac{A\beta_2}{4\alpha^3} \,, \qquad (126)
$$

so one fit constraint is lost (or deeply hidden) if we use the kaon mass to represent the strange mass.

Finally, we want to relate the partially quenched fit to the unitary results, on our trajectory $\frac{1}{3}(2m_l + m_s) = m_0$. If we use bare masses as our coordinates, we do this by using the substitutions

$$
\delta\mu_l \to \delta m_l \,, \qquad \delta\mu_s \to -2\delta m_l \,, \qquad (127)
$$

giving

$$\begin{aligned} M_\Delta &= M_0 + 3A\delta m_l + [B_0 + 3B_1]\delta m_l^2 \\ M_{\Sigma^*} &= M_0 \qquad\qquad + [B_0 + 6B_1 + 9B_2]\delta m_l^2 \\ M_{\Xi^*} &= M_0 - 3A\delta m_l + [B_0 + 9B_1 + 9B_2]\delta m_l^2 \\ M_\Omega &= M_0 - 6A\delta m_l + [B_0 + 12B_1]\delta m_l^2 \,. \end{aligned} \tag{128}$$

However, if we use meson-based coordinates, such as eq. (121), the mapping back to the unitary result is more complicated,

$$\begin{aligned} y &\to x \\ z &\to -2x + \frac{3(\beta_0 + 4\beta_1)}{4\alpha^2} x^2 \,. \end{aligned} \tag{129}$$

The mapping from z, our measure of the strange quark mass, back to x is complicated by a second order term. The reason is clear. On our trajectory, the relation $2\delta m_l + \delta m_s = 0$ is made exactly true for bare lattice quark masses, while the meson mass relations $2M_\pi^2 + M_S^2 \approx$ const. or $2M_K^2 + M_\pi^2 \approx$ const. are only true to leading order. Thus in conclusion if we are considering the curvature terms it is definitely better to use (bare) lattice quark masses as the coordinates.

D The action

The particular clover action used here has a single iterated mild stout smearing, [30] for the hopping terms together with thin links for the clover term (this is an attempt to ensure that the fermion matrix does not become too extended). Together with the (tree level) Symanzik improved gluon action this gives

$$S = S_G + S_{Fu} + S_{Fd} + S_{Fs} \,, \tag{130}$$

with the gluon action

$$S_G = \frac{6}{g_0^2} \left\{ c_0 \sum_{Plaquette} \frac{1}{3} \mathrm{Re}\,\mathrm{Tr}(1 - U_{Plaquette}) + c_1 \sum_{Rectangle} \frac{1}{3} \mathrm{Re}\,\mathrm{Tr}(1 - U_{Rectangle}) \right\} , \tag{131}$$

and

$$\beta = \frac{6c_0}{g_0^2} = \frac{10}{g_0^2} \qquad \text{and} \quad c_0 = \frac{20}{12} \,,\ c_1 = -\frac{1}{12} \,. \tag{132}$$

For each flavour the Wilson–Dirac fermion action is

$$\begin{aligned} S_{Fq} = & \\ \sum_x \Bigg\{ & \frac{1}{2} \sum_\mu [\overline{q}(x)(\gamma_\mu - 1)\tilde{U}_\mu(x) q(x + a\hat{\mu}) - \overline{q}(x)(\gamma_\mu + 1)\tilde{U}_\mu^\dagger(x - a\hat{\mu}) q(x - a\hat{\mu})] \\ & + \frac{1}{2\kappa_q} \overline{q}(x) q(x) - \frac{1}{4} a c_{sw} \sum_{\mu\nu} \overline{q}(x) \sigma_{\mu\nu} F_{\mu\nu}(x) q(x) \Bigg\} \,, \end{aligned} \tag{133}$$

where F is the 'clover' field strength, necessary for $O(a)$-improvement. As the up and down quarks are always taken here as mass degenerate we have $\kappa_u = \kappa_d \equiv \kappa_l$.

To to keep the action highly local, the hopping terms use a stout smeared link ('fat link') with $\alpha = 0.1$ 'mild smearing' for the Dirac kinetic term and Wilson mass term,

$$\begin{aligned} \tilde{U}_\mu(x) &= \exp\{iQ_\mu(x)\}\, U_\mu(x) \\ Q_\mu &= \frac{\alpha}{2i}\left[V_\mu U_\mu^\dagger - U_\mu V_\mu^\dagger - \tfrac{1}{3}\mathrm{Tr}(V_\mu U_\mu^\dagger - U_\mu V_\mu^\dagger)\right] , \end{aligned} \tag{134}$$

where $V_\mu(x)$ is the sum of all staples around $U_\mu(x)$. The clover term is built from thin links as it is already of length $4a$ and, as previously mentioned, we do not want the fermion matrix to become too extended. Stout smearing is analytic and so a derivative can be taken (so the HMC force is well defined) and also allows for perturbative expansions [31].

The clover coefficient, c_{sw}, has recently been non-perturbatively (NP) found, [19], by requiring that the axial Ward identity (WI) quark mass determined in several different ways is the same. A sensitive way of achieving this is the Schrödinger functional, or SF, formalism. Further details of our results may be found in [19]. c_{sw} is determined for 3 mass degenerate or $SU(3)$ flavour symmetric quarks (where $\kappa_l = \kappa_s \equiv \kappa_0$) in the chiral limit. A 5th order polynomial in g_0^2 interpolating between the numerically determined $c_{sw}(g_0)$ points was found to be, [19]

$$c_{sw}^*(g_0) = 1 + 0.269041\, g_0^2 + 0.29910\, g_0^4 - 0.11491\, g_0^6 - 0.20003\, g_0^8 + 0.15359\, g_0^{10} . \tag{135}$$

(This interpolation function is constrained to reproduce the $O(g_0^2)$ perturbative results, [31], in the $\beta \to \infty$ limit and therefore has four free fit parameters.) We take this result to define c_{sw} for a given β.

Improving one on-shell quantity to $O(a^2)$ (here the axial WI quark mass) fixes $c_{sw}(g_0^2)$ and then all masses are automatically improved to $O(a^2)$,

$$\frac{m_H}{m_{H'}} = \# + O(a^2) , \tag{136}$$

rather than just to $O(a)$. Operators in general require further $O(a)$ operators together with associated improvement coefficients to ensure $O(a)$–improvement for physical on-shell quantities.

This determination of c_{sw} via the Schrödinger Functional formalism also provides an estimate for the critical κ_0, [19], of

$$\begin{aligned} \kappa_{0;c}(g_0) &= \frac{1}{8}\left[1 + 0.002391\, g_0^2 + 0.0122470\, g_0^4 - 0.0525676\, g_0^6 \right. \\ &\qquad \left. + 0.0668197\, g_0^8 - 0.0242800\, g_0^{10}\right] . \end{aligned} \tag{137}$$

(Again this interpolation function is constrained to reproduce the $O(g_0^2)$ perturbative results, [31], in the $\beta \to \infty$ limit.) The errors are estimated to be about 0.4% at $\beta = 14.0$ rising to 0.15% at $\beta = 5.10$.

The simulations only need knowledge of c_{sw} to proceed; however it is useful to check consistency between different determinations of $\kappa_{0;c}$ (via the Schrödinger functional or the pseudoscalar mass). For $\beta = 5.50$ then using eq. (137) we find $\kappa_{0;c} = 0.120996$ (the direct simulation result is $\kappa_{0;c} = 0.121125(330)$, [19]). This is to be compared with the estimation in section 8.2 of $\kappa_{0;c} = 0.121069(25)$, which is quite close. (It should also be noted that different determinations should only agree up to $O(a)$ effects.)

E Hadron masses

We collect here in Tables 14 – 18 and 19 – 22 values of the pseudoscalar octet, vector octet, baryon octet and baryon decuplet masses for $\kappa_0 = 0.12090$ and $\kappa_0 = 0.12092$ respectively. In Tables 23 – 25 we give the ratios (i.e. hadron octet or decuplet masses normalised with their centre of mass). The data sets are roughly $\sim O(2000)$ trajectories for the $24^3 \times 48$ lattices and $\sim O(1500)$ trajectories for the $32^3 \times 64$ lattices for the results based on $\kappa_0 = 0.12090$ and lower for the comparison results. The errors are all taken from a bootstrap analysis of the ratio (which often enables a smaller error to be given for the ratios than simply using error propagation).

κ_0	$N_S^3 \times N_T$	aM_π	aM_ρ	aM_N	aM_Δ
0.12000	$16^3 \times 32$	0.4908(17)	0.6427(23)	0.9612(42)	1.048(6)
0.12030	$16^3 \times 32$	0.4026(19)	0.5635(38)	0.8374(74)	0.9414(107)
0.12050	$24^3 \times 48$	0.3375(24)	0.4953(47)	0.7201(83)	0.8216(89)
0.12080	$24^3 \times 48$	0.2260(10)	0.3903(55)	0.5417(68)	0.6415(99)
0.12090	$24^3 \times 48$		see Tables 15 – 18		
0.12090	$32^3 \times 64$		see Tables 15 – 18		
0.12092	$24^3 \times 48$		see Tables 19 – 22		
0.12095	$32^3 \times 64$	0.1506(9)	0.3095(54)	0.4321(75)	0.5539(110)

Table 14: The results for the hadrons on the symmetric line, aM_π, aM_ρ, aM_N and aM_Δ for $(\beta, c_{sw}, \alpha) = (5.50, 2.65, 0.1)$.

(κ_l, κ_s)	aM_π	aM_K	aM_{η_s}
	$24^3 \times 48$		
(0.120830, 0.121040)	0.1933(6)	0.1688(7)	0.1391(11)
(0.120900, 0.120900)	0.1779(6)	0.1779(6)	0.1779(6)
(0.120950, 0.120800)	0.1661(8)	0.1845(7)	0.2011(7)
(0.121000, 0.120700)	0.1515(10)	0.1898(8)	0.2209(6)
(0.121040, 0.120620)	0.1406(8)	0.1949(6)	0.2361(5)
	$32^3 \times 64$		
(0.120900, 0.120900)	0.1768(7)	0.1768(7)	0.1768(7)
(0.121040, 0.120620)	0.1349(5)	0.1896(4)	0.2320(4)
(0.121095, 0.120512)	0.1165(7)	0.1962(4)	0.2518(3)
(0.121145, 0.120413)	0.09698(93)	0.2017(5)	0.2684(3)

Table 15: The results for the pseudoscalar octet mesons: aM_π, aM_K and aM_{η_s} for $(\beta, c_{sw}, \alpha) = (5.50, 2.65, 0.1)$ where $\kappa_0 = 0.12090$.

(κ_l, κ_s)	aM_ρ	aM_{K^*}	aM_{ϕ_s}
	$24^3 \times 48$		
(0.120830, 0.121040)	0.3460(22)	0.3335(30)	0.3198(48)
(0.120900, 0.120900)	0.3494(25)	0.3494(25)	0.3494(25)
(0.120950, 0.120800)	0.3400(40)	0.3473(32)	0.3546(27)
(0.121000, 0.120700)	0.3364(43)	0.3517(30)	0.3663(20)
(0.121040, 0.120620)	0.3270(50)	0.3484(28)	0.3701(18)
	$32^3 \times 64$		
(0.120900, 0.120900)	0.3401(58)	0.3401(58)	0.3401(58)
(0.121040, 0.120620)	0.3125(41)	0.3379(23)	0.3632(16)
(0.121095, 0.120512)	0.3130(50)	0.3433(22)	0.3749(13)
(0.121145, 0.120413)	0.3152(63)	0.3487(22)	0.3880(12)

Table 16: The results for the vector octet mesons: aM_ρ, aM_{K^*} and aM_{ϕ_s} for $(\beta, c_{sw}, \alpha) = (5.50, 2.65, 0.1)$ where $\kappa_0 = 0.12090$.

(κ_l, κ_s)	aM_N	aM_Λ	aM_Σ	aM_Ξ
$24^3 \times 48$				
(0.120830, 0.121040)	0.4976(25)	0.4859(43)	0.4791(31)	0.4679(39)
(0.120900, 0.120900)	0.4811(33)	0.4811(33)	0.4811(33)	0.4811(33)
(0.120950, 0.120800)	0.4737(68)	0.4794(58)	0.4871(55)	0.4938(48)
(0.121000, 0.120700)	0.4648(46)	0.4815(49)	0.4910(36)	0.5055(28)
(0.121040, 0.120620)	0.4466(66)	0.4810(57)	0.4843(42)	0.5068(32)
$32^3 \times 64$				
(0.120900, 0.120900)	0.4746(66)	0.4746(66)	0.4746(66)	0.4746(66)
(0.121040, 0.120620)	0.4271(52)	0.4524(44)	0.4710(35)	0.4910(24)
(0.121095, 0.120512)	0.4062(61)	0.4498(62)	0.4667(37)	0.4971(22)
(0.121145, 0.120413)	0.4022(115)	0.4582(77)	0.4755(45)	0.5105(22)

Table 17: The results for the octet baryons: aM_N, aM_Λ, aM_Σ and aM_Ξ for $(\beta, c_{sw}, \alpha) = (5.50, 2.65, 0.1)$ where $\kappa_0 = 0.12090$.

(κ_l, κ_s)	aM_Δ	aM_{Σ^*}	aM_{Ξ^*}	aM_Ω
$24^3 \times 48$				
(0.120830, 0.121040)	0.5906(73)	0.5801(89)	0.5685(114)	0.5548(151)
(0.120900, 0.120900)	0.5933(88)	0.5933(88)	0.5933(88)	0.5933(88)
(0.120950, 0.120800)	0.5817(55)	0.5895(48)	0.5973(43)	0.6050(38)
(0.121000, 0.120700)	0.5883(101)	0.6006(77)	0.6133(61)	0.6262(51)
(0.121040, 0.120620)	0.5483(137)	0.5679(90)	0.5902(64)	0.6108(48)
$32^3 \times 64$				
(0.120900, 0.120900)	0.5895(169)	0.5895(169)	0.5895(169)	0.5895(169)
(0.121040, 0.120620)	0.5552(85)	0.5775(57)	0.5991(42)	0.6210(34)
(0.121095, 0.120512)	0.5288(193)	0.5610(105)	0.5838(63)	0.6115(40)
(0.121145, 0.120413)	0.5047(219)	0.5551(98)	0.6019(50)	0.6421(29)

Table 18: The results for the decuplet baryons: aM_Δ, aM_{Σ^*}, aM_{Ξ^*} and aM_Ω for $(\beta, c_{sw}, \alpha) = (5.50, 2.65, 0.1)$ where $\kappa_0 = 0.12090$.

(κ_l, κ_s)	aM_π	aM_K	aM_{η_s}
	$24^3 \times 48$		
(0.120920, 0.120920)	0.1694(9)	0.1694(9)	0.1694(9)
	$32^3 \times 64$		
(0.120500, 0.120661)	0.1280(6)	0.1813(5)	0.2221(4)

Table 19: The results for the pseudoscalar octet mesons: aM_π, aM_K and aM_{η_s} for $(\beta, c_{sw}, \alpha) = (5.50, 2.65, 0.1)$ where $\kappa_0 = 0.12092$.

(κ_l, κ_s)	aM_ρ	aM_{K^*}	aM_{ϕ_s}
	$24^3 \times 48$		
(0.120920, 0.120920)	0.3404(44)	0.3404(44)	0.3404(44)
	$32^3 \times 64$		
(0.120900, 0.120661)	0.3161(38)	0.3354(22)	0.3564(16)

Table 20: The results for the vector octet mesons: aM_ρ, aM_{K^*} and aM_{ϕ_s} for $(\beta, c_{sw}, \alpha) = (5.50, 2.65, 0.1)$ where $\kappa_0 = 0.12092$.

(κ_l, κ_s)	aM_N	aM_Λ	aM_Σ	aM_Ξ
	$24^3 \times 48$			
(0.120920, 0.120920)	0.4725(39)	0.4725(39)	0.4725(39)	0.4725(39)
	$32^3 \times 64$			
(0.120500, 0.120661)	0.4127(42)	0.4444(35)	0.4580(31)	0.4798(22)

Table 21: The results for the octet baryons: aM_N, aM_Λ, aM_Σ and aM_Ξ for $(\beta, c_{sw}, \alpha) = (5.50, 2.65, 0.1)$ where $\kappa_0 = 0.12092$.

(κ_l, κ_s)	aM_Δ	aM_{Σ^*}	aM_{Ξ^*}	aM_Ω
	$24^3 \times 48$			
(0.120920, 0.120920)	0.5790(97)	0.5790(97)	0.5790(97)	0.5790(97)
	$32^3 \times 64$			
(0.120500, 0.120661)	0.5457(108)	0.5607(72)	0.5800(51)	0.6005(40)

Table 22: The results for the decuplet baryons: aM_Δ, aM_{Σ^*}, aM_{Ξ^*} and aM_Ω for $(\beta, c_{sw}, \alpha) = (5.50, 2.65, 0.1)$ where $\kappa_0 = 0.12092$.

(κ_l, κ_s)	M_ρ/X_ρ	M_{K^*}/X_ρ	M_{ϕ_s}/X_ρ
$24^3 \times 48$			
(0.120830, 0.121040)	1.025(2)	0.9877(12)	0.9470(155)
(0.120900, 0.120900)	1.0	1.0	1.0
(0.120950, 0.120800)	0.9859(22)	1.007(1)	1.028(6)
(0.121000, 0.120700)	0.9706(34)	1.015(2)	1.057(12)
(0.121040, 0.120620)	0.9488(50)	1.026(3)	1.102(6)
$32^3 \times 64$			
(0.120900, 0.120900)	1.0	1.0	1.0
(0.121040, 0.120620)	0.9485(54)	1.026(3)	1.102(7)
(0.121095, 0.120512)	0.9394(79)	1.030(4)	1.125(8)
(0.121145, 0.120413)	0.9338(111)	1.033(6)	1.149(9)

Table 23: Ratio results for the vector octet mesons: M_ρ/X_ρ, M_{K^*}/X_ρ and M_{ϕ_s}/X_ρ for $(\beta, c_{sw}, \alpha) = (5.50, 2.65, 0.1)$ where $\kappa_0 = 0.12090$.

(κ_l, κ_s)	M_N/X_N	M_Λ/X_N	M_Σ/X_N	M_Ξ/X_N
$24^3 \times 48$				
(0.120830, 0.121040)	1.033(2)	1.009(6)	0.9949(13)	0.9717(26)
(0.120900, 0.120900)	1.0	1.0	1.0	1.0
(0.120950, 0.120800)	0.9769(33)	0.9887(84)	1.005(1)	1.018(3)
(0.121000, 0.120700)	0.9543(32)	0.9885(77)	1.008(2)	1.038(3)
(0.121040, 0.120620)	0.9319(56)	1.004(7)	1.011(2)	1.058(4)
$32^3 \times 64$				
(0.120900, 0.120900)	1.0	1.0	1.0	1.0
(0.121040, 0.120620)	0.9224(48)	0.9770(73)	1.017(3)	1.060(4)
(0.121095, 0.120512)	0.8949(92)	0.9863(113)	1.020(4)	1.085(9)
(0.121145, 0.120413)	0.8691(154)	0.9902(154)	1.028(7)	1.103(10)

Table 24: Ratio results for the octet baryons: M_N/X_N, M_Λ/X_N, M_Σ/X_N and M_Ξ/X_N for $(\beta, c_{sw}, \alpha) = (5.50, 2.65, 0.1)$ where $\kappa_0 = 0.12090$.

(κ_l, κ_s)	M_Δ/X_Δ	M_{Σ^*}/X_Δ	M_{Ξ^*}/X_Δ	M_Ω/X_Δ
$24^3 \times 48$				
(0.120830, 0.121040)	1.021(6)	1.003(2)	0.9824(44)	0.9588(121)
(0.120900, 0.120900)	1.0	1.0	1.0	1.0
(0.120950, 0.120800)	0.9868(14)	1.000(0)	1.013(2)	1.026(3)
(0.121000, 0.120700)	0.9790(42)	0.9993(24)	1.020(6)	1.042(8)
(0.121040, 0.120620)	0.9634(72)	0.9978(53)	1.037(11)	1.073(14)
$32^3 \times 64$				
(0.120900, 0.120900)	1.0	1.0	1.0	1.0
(0.121040, 0.120620)	0.9620(43)	1.001(3)	1.038(6)	1.076(9)
(0.121095, 0.120512)	0.9538(130)	1.008(11)	1.045(21)	1.092(26)
(0.121145, 0.120413)	0.9168(153)	1.008(16)	1.093(26)	1.166(31)

Table 25: Ratio results for the decuplet baryons: M_Δ/X_Δ, M_{Σ^*}/X_Δ, M_{Ξ^*}/X_Δ and M_Ω/X_Δ for $(\beta, c_{sw}, \alpha) = (5.50, 2.65, 0.1)$ where $\kappa_0 = 0.12090$.

References

[1] W. Bietenholz, V. Bornyakov, N. Cundy, M. Göckeler, R. Horsley, A. D. Kennedy, W. G. Lockhart, Y. Nakamura, H. Perlt, D. Pleiter, P. E. L. Rakow, A. Schäfer, G. Schierholz, A. Schiller, H. Stüben and J. M. Zanotti, [QCDSF–UKQCD Collaboration], *Phys. Lett.* **B690** (2010) 436 [arXiv:1003.1114[hep-lat]].

[2] M. Göckeler, R. Horsley, A. C. Irving, D. Pleiter, P. E. L. Rakow, G. Schierholz and H. Stüben, [QCDSF–UKQCD Collaboration], *Phys. Lett.* **B639** (2006) 307 [arXiv:hep-ph/0409312].

[3] P. E. L. Rakow, *Nucl. Phys. Proc. Suppl.* **140** (2005) 34 [arXiv:hep-lat/0411036].

[4] A. Skouroupathis and H. Panagopoulos, *Phys. Rev.* **D76** (2007) 094514; Erratum-ibid. **D78** (2008) 119901 [arXiv:0707.2906[hep-lat]].

[5] A. Skouroupathis and H. Panagopoulos, *Phys. Rev.* **D79** (2009) 094508 [arXiv:0811.4264[hep-lat]].

[6] P. W. Atkins, M. S. Child and C. S. G. Phillips, *Tables for Group Theory*, Oxford, 1970.

[7] S. Capitani, M. Göckeler, R. Horsley, P. E. L. Rakow and G. Schierholz, *Phys. Lett.* **B468** (1999) 150-160 [arXiv:hep-lat/9908029].

[8] T. Bhattacharya, R. Gupta, W. Lee, S. R. Sharpe and J. M. S. Wu, *Phys. Rev.* **D73** (2006) 034504 [arXiv:hep-lat/0511014].

[9] S. Coleman and S. L. Glashow, *Phys. Rev. Lett.* **6** (1961) 423.

[10] M. Gell-Mann, *Phys. Rev.* **125** (1962) 1067.

[11] S. Okubo, *Prog. Theor. Phys.* **27** (1962) 949.

[12] W. Pfeifer, *The Lie Algebras su(N), An Introduction*, Birkhäuser, Basel, 2003.

[13] W. Greiner and B. Müller, *Quantum Mechanics: Symmetries*, Springer, 1989.

[14] S. Gasiorowicz, *Elementary Particle Physics*, John Wiley & Sons, New York, 1966.

[15] B. C. Tiburzi and A. Walker-Loud, *Nucl. Phys.* **A748** 513 (2005) 513 [arXiv:hep-lat/0407030].

[16] A. Walker-Loud, *Nucl. Phys.* **A747** (2005) 476 [arXiv:hep-lat/0405007].

[17] QCDSF–UKQCD Collaboration, in preparation.

[18] C. Allton, D. J. Antonio, Y. Aoki, T. Blum, P. A. Boyle, N. H. Christ, S. D. Cohen, M. A. Clark, C. Dawson, M. A. Donnellan, J.M. Flynn, A. Hart, T. Izubuchi, A. Jüttner, C. Jung, A. D. Kennedy, R. D. Kenway, M. Li, S. Li, M. F. Lin, R. D. Mawhinney, C. M. Maynard, S. Ohta, B. J. Pendleton, C. T. Sachrajda, S. Sasaki, E. E. Scholz, A. Soni, R. J. Tweedie, J. Wennekers, T. Yamazaki and J. M. Zanotti, [RBC–UKQCD Collaboration] *Phys. Rev.* **D78** (2008) 114509 [arXiv:0804.0473[hep-lat]].

[19] N. Cundy, M. Göckeler, R. Horsley, T. Kaltenbrunner, A. D. Kennedy, Y. Nakamura, H. Perlt, D. Pleiter, P. E. L. Rakow, A. Schäfer, G. Schierholz, A. Schiller, H. Stüben and J. M. Zanotti, [QCDSF–UKQCD Collaboration] *Phys. Rev.* **D79** (2009) 094507 [arXiv:0901.3302[hep-lat]].

[20] Y. Nakamura and H. Stüben, *PoS(Lattice 2010)* **040** [arXiv:1011.0199[hep-lat]].

[21] M. Lüscher, S. Sint, R. Sommer and P. Weisz, *Nucl. Phys.* **B478** (1996) 365 [arXiv:hep-lat/9605038].

[22] T. Bakeyev, M. Göckeler, R. Horsley, D. Pleiter, P. E. L. Rakow, G. Schierholz and H. Stüben, *Phys. Lett.* **B580** (2004) 197 [arXiv:hep-lat/0305014].

[23] C. R. Allton, C. T. Sachrajda, R. M. Baxter, S. P. Booth, K. C. Bowler, S. Collins, D. S. Henty, R. D. Kenway, B. J. Pendleton, D. G. Richards, J. N. Simone, A. D. Simpson and B. E. Wilkes, *Phys. Rev.* **D47** (1993) 5128, [arXiv:hep-lat/9303009].

[24] C. Best, M. Göckeler, R. Horsley, E.-M. Ilgenfritz, H. Perlt, P. Rakow, A. Schäfer, G. Schierholz, A. Schiller and S. Schramm, *Phys. Rev.* **D56** (1997) 2743, [arXiv:hep-lat/9703014].

[25] A. Billoire, E. Marinari and R. Petronzio, *Nucl. Phys.* **B251[FS13]** (1985) 141.

[26] M. Göckeler, R. Horsley, M. Ilgenfritz, H. Perlt, P. Rakow, G. Schierholz and A. Schiller, *Nucl. Phys. Proc. Suppl.* **42** (1995) 337 [arXiv:hep-lat/9412055].

[27] M. Göckeler, R. Horsley, D. Pleiter, P. E. L. Rakow and G. Schierholz, *Phys. Rev.* **D71**(2005) 114511 [arXiv:hep-ph/0410187].

[28] S. R. Beane, K. Orginos and M. J. Savage, [NPLQCD Collaboration], *Phys. Lett.* **B654** (2007) 20 [arXiv:hep-lat/0604013].

[29] K. Nakamura *et al.* (Particle Data Group), *J. Phys.* **G 37** (2010) 075021.

[30] C. Morningstar and M. J. Peardon, *Phys. Rev.* **D69** (2004) 054501 [arXiv:hep-lat/0311018].

[31] R. Horsley, H. Perlt, P. E. L. Rakow, G. Schierholz and A. Schiller, QCDSF Collaboration, *Phys. Rev.* **D78** (2008) 054504 [arXiv:0807.0345[hep-lat]].

[32] M. Göckeler, Ph. Hägler, R. Horsley, Y. Nakamura, D. Pleiter, P. E. L. Rakow, A. Schäfer, G. Schierholz, H. Stüben, F. Winter and J. M. Zanotti, [QCDSF–UKQCD Collaboration], *PoS(Lattice 2010)* **165** arXiv:1101.2806[hep-lat].

[33] M. Göckeler, Ph. Hägler, R. Horsley, Y. Nakamura, D. Pleiter, P. E. L. Rakow, A. Schäfer, G. Schierholz, H. Stüben, F. Winter and J. M. Zanotti, [QCDSF–UKQCD Collaboration], *PoS(Lattice 2010)* **163** arXiv:1102.3407[hep-lat].

[34] P. A. Boyle, *Comp. Phys. Comm.* **180** (2009) 2739.